8-2021

ADVANCEMENT OF A 3D COMPUTATIONAL PHANTOM AND ITS AGE SCALING METHODOLOGIES FOR RETROSPECTIVE DOSE RECONSTRUCTION STUDIES

Aashish Gupta

ADVANCEMENT OF A 3D COMPUTATIONAL PHANTOM AND ITS AGE SCALING METHODOLOGIES FOR RETROSPECTIVE DOSE RECONSTRUCTION STUDIES

by

Aashish Chandra Gupta, B.S.

APPROVED:

_____
Rebecca M. Howell, Ph.D.
Advisory Professor

_____
Stephen F. Kry, Ph.D.

_____
Choonsik Lee, Ph.D.

_____
Peter A. Balter, Ph.D.

_____
David S. Followill, Ph.D.

_____
James P. Long, Ph.D.

APPROVED:

_____
Dean, The University of Texas
MD Anderson Cancer Center UTHealth Graduate School of Biomedical Science

ADVANCEMENT OF A 3D COMPUTATIONAL PHANTOM AND ITS AGE SCALING METHODOLOGIES FOR RETROSPECTIVE DOSE RECONSTRUCTION STUDIES

A

THESIS

Presented to the Faculty of

The University of Texas

MD Anderson Cancer Center UTHealth

Graduate School of Biomedical Sciences

in Partial Fulfillment

of the Requirements

for the Degree of

MASTER OF SCIENCE

by

Aashish Chandra Gupta, B.S.

Houston, Texas

August 2021

Dedication

Dedicated to my parents, Dinesh and Punam, and my brother, Max, for their endless love, support, and encouragements

Acknowledgments

First and foremost, I want to thank my advisor, Professor Rebecca Maureen Howell, for all the support and guidance you have given me in the last three years. Thank you for recognizing my research potential and always believing in my vision for the project. Beyond your guidance in my project, you have also set a marvelous example of mentorship and have inspired me to be a mentor like you in the future.

Thank you to my committee members: Drs. Choonsik Lee, Stephen F. Kry, Peter A. Balter, David S. Followill, and James P. Long, for your inputs and contributions to this project and manuscripts. Thank you for your willingness to always meet with me and provide ideas for the project. A special thanks to Dr. Lee for providing us various software and one of the best computational phantom libraries for the project. Thank you for your promptness and willingness to guide me in developing phantom study even when I had made several last-minute requests.

Thank you to Cameroon Ditty for helping us with phantom implementation in RayStation. Thank you to Keith T. Griffin for providing us the DICOM RT generator software. Thank you to Dr. Tucker Netherton for helping us with the segmentations of vertebral bodies. A special thanks to Susan Smith for being a fabulous mentor. You did not only help me achieve my research goals but also helped me to succeed in graduate school in overall. Thank you to Constance Owens and Suman Shrestha for all the contribution, support, and encouragement in the last three years. Both of you have contributed in countless ways, which have enabled us to accomplish our research goals smoothly. A special thanks to Constance for always being there for anything.

Thank you, Dr. Richard E. Wendt III, for being an excellent mentor and a role model to me. Words cannot convey enough gratitude for everything you have done for me since I was an undergraduate student. Thank you, Anne Baronitis for always checking up on me during the pandemic. Thank you, Frances Quintana, for always being there to help.

Finally, thank you to my family and friends for your endless love, support, and encouragement, allowing me to accomplish my goals and reach this far.

Abstract

ADVANCEMENT OF A 3D COMPUTATIONAL PHANTOM AND ITS AGE SCALING METHODOLOGIES FOR RETROSPECTIVE DOSE RECONSTRUCTION STUDIES

Aashish Chandra Gupta, B.S.

Advisory Professor: Rebecca M. Howell, Ph.D.

We have used a 3D age-scalable computational phantom for over two decades for retrospective dose reconstruction studies of childhood cancer survivors (CCS) treated with 2D historic radiotherapy (RT). However, our phantom and its age scaling functions (ASF) must be updated so that it can be used in studies that include survivors treated with contemporary RT. We aimed to implement our phantom and its age scaling functions in DICOM format and determine the feasibility of applying our ASFs to accurately scale the whole-body CT-based anatomies.

In the implementation study, we developed Python scripts that model the phantom and ASFs in a treatment planning system (TPS). We validated the implementation by comparing several geometric and anthropometric parameters with reference datasets. We then conducted a dosimetric analysis to determine the accuracy of dose calculation using our phantom. In the feasibility study, we downscaled various computed tomography (CT)-based

phantoms from the University of Florida/National Cancer Institute (UF/NCI) phantom library to arbitrary ages. We quantified the geometric accuracy of scaling by comparing several overlaps, distance, and anthropometric parameters of the scaled phantom with reference datasets. We also assessed the dosimetric impact of ASFs by quantifying the difference in dose from standard Wilms' tumor RT plan simulated on exact age-scaled and nearest age-matched phantom while using the same field size and anatomical landmark dependent field size in two different scenarios.

This study showed that phantoms were implemented in DICOM format within 3% of points/volume of our original phantoms. The heights and dosimetric accuracy were within 7% of ground-truth values. In the feasibility study, overlap metrics showed "good" agreement for most cases except pancreas and kidneys. The maximum displacement of 4.1cm was obtained in the scaled liver. In both implementation and feasibility studies, organ masses were smaller than reference masses in general. A difference of 6% and 1.3Gy was obtained for percent volume $\geq$ 15Gy (V_{15}) and mean dose, respectively, across two phantom categories when the same field size was used. Both metrics were significantly different ($p<0.05$) for partially in-beam organs when field size varied. Overall, our results show that phantom and ASFs can be accurately used in TPS for modern RT studies, and our ASFs can accurately scale whole-body CT-based anatomy.

Table of Contents

List of Illustrations

List of Tables

Chapter 1: Introduction

1. Background to the Problem

The advancements of radiation therapy (RT) treatment techniques have increased the survival rate of cancer patients over the last few decades, however, RT modalities are associated with dose to non-target organs/organs at risk (OAR) at the same time (Kry *et al* 2017). The dose to OARs depends on the proximity of the organ to the target volume. Organs that are completely in-beam or partially in-beam receive varying degrees of unwanted radiation, largely depending on their proximity to the target volume. Organs that are entirely out of beam receive lesser amounts of unwanted radiation due to stray radiation originating from linac head leakage, collimator scatters, and patient scatters (Kry *et al* 2017, Xu *et al* 2008). The dose received by these OARs increases the risk of developing early and late effects/toxicity in these organs (Kry *et al* 2017). It has been estimated that 1% of the cancer survivors will develop RT-related subsequent neoplasm (SNM), which corresponds to approximately 150,000 patients (De Gonzalez *et al* 2011). In the case of childhood cancer survivors (CCS) treated with radiation therapy (RT), the survivors are at higher risk to develop late effects as they have greater tissue sensitivity to radiation (Kutanzi *et al* 2016), a longer life expectancy, and a greater survival rate than an adult (Armstrong *et al* 2016, Turcotte *et al* 2017, Gibson *et al* 2018).

1.1 RT epidemiologic studies

The risk of developing late effects is investigated in radiation epidemiologic studies (also known as late effects studies) where doses from RT to OARs are correlated with late effects in

those organs in long-term cancer survivors. Because late effects occur years and often decades after treatment, survivor cohorts often include survivors treated in the pre-computed tomography era of RT. Thus, organ doses are not available in their historic RT records and must be reconstructed in retrospect using surrogate anatomy. This is typically done using established dose reconstruction methods (Stovall *et al* 2006, Howell *et al* 2019), briefly summarized here.

We first begin by abstracting RT treatment plan from the cancer survivor cohort (N>10,000), and then we reconstruct RT fields on surrogate anatomy to estimate dose to OARs (Stovall *et al* 2006, Howell *et al* 2019). The abstraction usually involves coding of anthropometric parametric and RT plans of the survivor. If the cohorts include survivors treated in the pre-CT era, then parameters such as age, height and weight (sporadically available), sex, date, prescription dose, beam energy, orientation, field size, anatomical landmarks, and organs proximity to the fields are available (Howell *et al* 2019). These parameters are used to reconstruct the dose on the surrogate anatomy. If the cohort includes survivors treated with contemporary RT such as 3D conformal RT, intensity, volumetric modulated RT (IMRT and VMAT) and particle therapy, then a survivor CT scan with an RT plan is available. However, partial CT scans are available in most cases where information is limited to anatomy near the target volume. Therefore, surrogate anatomy for missing organs/body regions is combined with a partial CT scan to estimate the organ dose. Since doses are reconstructed in retrospect in both cases, the success of such studies is heavily dependent on the accuracy, suitability, and efficacy of dose reconstruction methods

and the type of surrogate anatomy used in the studies as associated uncertainty could result in a large error in risk assessments (Xu *et al* 2008, Vũ Bezin *et al* 2017).

There are two major approaches that are used to reconstruct organ doses from the stray radiation: (1) anthropometric phantom approach, (2) computational approaches (Stovall *et al* 2006, Howell *et al* 2019, Kry *et al* 2017, Xu *et al* 2008). In the anthropometric phantom approach, organ doses are measured using phantoms such as Alderson RANDO phantoms which consist of contiguous plastic slabs of tissue equivalent materials for varying the shape and the size. The dosimeters such as Thermoluminiscents detectors (TLD) are placed at different distances and depths, and the phantoms are irradiated using treatment parameters to estimate the dose (Stovall *et al* 2006). There exist several limitations that preclude its use in large cohorts of cancer survivors. First of all, the anthropometrics phantoms are limited to specific ages, and the phantom slabs have limited thickness and number per body region, limiting the variation in shape. Further, it is not feasible to perform the physical experiments using phantoms for all survivors in large cohorts. In computational approaches, a treatment planning system (TPS) can be used to estimate in-beam or partially in-beam organ dose, but the accuracy decreases as the distance between out-of-field organ and main treatment field increases (Kry *et al* 2017). It has been found that TPS exhibits up to 30% error in organ doses that are 3cm from the field edges (Howell *et al* 2010b). The Monte Carlo methods are one of the feasible options in which different treatment scenarios and patient geometrical models can be simulated. However, the models must be validated with the machines used for treatment (Kry *et al* 2017) which is not feasible to conduct for each survivor in large cohorts. Considering the limitations mentioned above, the most viable option for large cohorts is

analytical dose calculation models combined with 3D computational phantoms. The analytical models consist of mathematical formulation and measurement data for different field sizes, beam energy, depth, orientation, etc., which are used when RT fields are reconstructed on computational phantoms to reconstruct dose to OARs (Stovall *et al* 2006, Howell *et al* 2019, Kry *et al* 2017).

1.2 Computational phantoms

There are different categories of computational phantoms that have the potential for use in late effects studies. The first and the simplest class is stylized phantoms which is also the most widely used phantom type for CCS treated in the pre-CT era (Howell *et al* 2019). Stylized phantoms consist of simple geometrical shapes that represent organs and body regions (Xu 2014). The geometrical structures are described by quadratic equations, allowing them to be scaled to match various anthropometric parameters (Kry *et al* 2017, Zaidi and Tsui 2009, Xu 2014). However, the main limitation of these phantoms is the deviation from realistic and complex human anatomy, which could introduce uncertainty in organ dose estimation if the dose reconstruction method relies on the organ shape. The anatomical realism has been addressed up to an appreciable extent in the next category known as Voxel phantoms. In this type, the voxels defining organs and body regions are obtained by segmenting patient CT/MRI scans (Lee *et al* 2010, Zaidi and Tsui 2009, Xu 2014). Voxels defining a particular organ are given the same identification numbers. Although voxel phantoms are anatomically more realistic than stylized phantoms, they cannot be scaled to different heights, ages, weights, etc., which results in errors up to 150% in some cases when used instead of stylized phantoms (Kry *et al* 2017, Lee *et al* 2006). The most advanced and most realistic category of

the phantom is hybrid phantoms which combine anatomical realism of voxel phantoms with the mathematical surface equations of the stylized phantoms (Bolch *et al* 2010). There are several hybrid phantom libraries which include reference size, body-size dependent (height and weight dependent), patient-specific, and percentile-specific phantoms and can be scaled to match various anthropometric parameters but the time required to scale each phantom ranges up to 20 minutes which could result in the longer calculation time for large cohorts. Another limitation is that phantoms are available at discrete ages (e.g. newborn, 1, 5, 10, 15, adult) or at discrete heights or discrete weights due to which nearest available age or height or weight are used when the phantom of exact parameter for survivors is unavailable. The could result in uncertainty organ dose and risk-assessment studies.

2. MD Anderson Late Effects Group Computational Phantoms and Statement of the Problem

The Radiation Dosimetry Service (RDS) at UT MD Anderson Cancer Center developed a 3D age-scalable computational phantom over three decades ago, which has been used in more than 120 studies for retrospective dose reconstruction of CCS treated with 2D RT plans (Howell *et al* 2019). This phantom was modeled initially in FORTRAN and can be scaled to any arbitrary age using non-uniform body region-specific 3D age-scaling functions (ASFs). The phantom consists of 5 rectangular cuboids representing the head, neck, trunk, legs, arms, body regions, and over 20 organs. Each body region and organ is represented by 3D points, and doses are predicted by calculating the dose to individual points using several reconstruction methods as described by Stovall *et al* (2006) and Howell *et al* (2019). The availability of robust and fast age-scaling methodologies makes this phantom suitable for the dose reconstruction studies of large retrospective cohorts.

The modern cohorts of CCS are treated with contemporary RT modalities such as 3D CRT, IMRT, and VMAT, where survivor's treatment plans are present in Digital Imaging and Communication in Medicine (DICOM) Standard CT images. In most cases, the survivors have partial CT scans that only span the anatomy in the proximity of the target volume. To estimate dose to organs that are not present in the CT image, one must calculate dose retrospectively using the alternative dose reconstruction methods as TPS calculated doses are inaccurate for out-of-field organs. Furthermore, in some longitudinal studies, whole-body CT scans of survivors could be available, which will need to be downscaled and fused with a partial CT scan of the survivor at different timepoints. Our dose reconstruction method and computational infrastructure can accurately estimate dose in the previously mentioned cases, provided that the computational phantom and its ASFs are accurately implemented in the DICOM format.

3. Project Objective

The overall objective of this project was to make our phantom and its ASFs compatible with survivors treated with modern RT and determine the feasibility and accuracy of scaling whole-body CT-based anatomies using our ASFs. Specifically, we first aimed to implement and validate our phantom and its ASFs in DICOM format. Secondly, we implemented and validated our ASFs to determine the feasibility of scaling whole-body CT-based anatomy to any arbitrary age. The implementation mentioned above, and validation will allow us to use our computational phantoms for cohorts treated with contemporary RT and the ASFs to scale any other whole-body CT-based anatomy, allowing us to use exact age-scaled phantoms in late-effects studies.

4. Organization of the Thesis

In Chapter 2 of the thesis, the details about the hypothesis, specific aims, and the projects within each aim are presented. In chapter 3, the implementation and validation of our computational phantom in the DICOM format are discussed. In chapter 4, the feasibility of scaling whole-body CT-based anatomy is discussed. In chapter 5, the general overview and future direction of the project are presented. In appendix A, the mathematical theory of scaling our computational phantom to 7.0-year-old is presented. In appendix B, the scaling of the arbitrary computational phantom using our ASFs through a graphical user interface (GUI) in the commercial treatment planning system is presented.

Chapter 2: Central Hypothesis and Specific Aims

1. Central Hypothesis

The central hypothesis of this thesis is that we can accurately convert our current phantom and its ASFs to DICOM format (within 3%) in a commercial TPS with the ability to scale our phantom and any CT based anatomy to any arbitrary age, i.e., infant through adult such that the phantom height across the age range agrees within 7% of the reference height data

2. Specific Aim 1: Implementation and Validation in the DICOM Format

Aim: Implement the phantom in DICOM format and establish the geometric accuracy in modeling of body regions and organs

Hypothesis: The computational phantom can be modeled in DICOM format within ± 3% of the FORTRAN phantom

Project 1.1: Develop a python script to implement the baseline FORTRAN phantom and its ASFs in DICOM format within TPS

Project 1.2: Validate the phantoms in DICOM format with FORTRAN phantom and reference data from Center for Disease Control and Prevention, and International Commission on Radiological Protection 89 report

Project 1.3: Investigate the feasibility of using phantom in DICOM format for dose calculation in commercial TPS and validate the organ dose with in-house dose calculation software

Specific Aim 1 is fully addressed in chapter 3: Development of an age-scalable 3D computational phantom in the DICOM format

3. Specific Aim 2: Feasibility of Scaling CT-Based Anatomy to Arbitrary Ages

Aim: Apply ASFs to scale the whole-body CT based anatomy to any arbitrary ages and validate scaling with ground-truth anatomy and reference data

Hypothesis: The ASFs can be used to scale whole-body CT-based anatomy to any arbitrary ages age within 7% of the CDC reported reference height. The Dice similarity coefficient (DSC) and mean distance agreement (MDA) of the scaled and ground-truth anatomy are within $\geq 70\%$ and within 5cm, respectively.

Project 2.1: Develop a python script to classify the whole-body CT based anatomy to head, neck, trunk, and leg body regions

Project 2.2: Apply the ASFs to scale whole-body CT based anatomy to any arbitrary age

Project 2.3: Validate the scaled anatomy with ground-truth anatomy and reference data from CDC and ICRP 89

Project 2.4: Apply ASFs to conduct a dose study to determine the difference in organ doses of exact age-scaled versus nearest age-matched phantoms

Specific Aim 2 is fully addressed in chapter 4: Scaling of whole-body computed tomography-based anatomy to any age.

Chapter 3: Development of an Age-Scalable 3D Computational Phantom in the DICOM Format

This chapter is based on the following peer-reviewed publication:

A.C. Gupta, S. Shrestha, C.A. Owens, S.A. Smith, Y. Qiao, R.E. Weathers., P.A. Balter, S.F. Kry, and R.M. Howell, "Development of an age-scalable 3D computational phantom in DICOM standard for late effects studies of childhood cancer survivors," Biomedical Physics and Engineering Express. Volume 6, Issue 6, pages 1-15.

This chapter describes the results of Specific Aim 1: Implement the phantom in DICOM format and establish the geometric accuracy in modeling of body regions and organs

1. Introduction

As mentioned in chapter 1, cancer survivors whose treatment included radiation therapy (RT) are at risk for developing RT-related late effects (≥5 years after diagnosis) (Travis *et al* 2011). Survivors of childhood cancer are at particularly high risk because of high survival rates (>84%) and long-life expectancy (Armstrong *et al* 2016, Turcotte *et al* 2017, Gibson *et al* 2018, Howlader *et al* 2019). Retrospective epidemiologic studies of cancer survivor cohorts investigate the relationship between RT dose to specific organs or body regions and the risk of subsequent late effects (Travis *et al* 2011). Such studies typically use computational

phantoms to retrospectively reconstruct doses throughout patients' bodies (Lee *et al* 2010, Travis *et al* 2011, Xie and Zaidi 2014, Howell *et al* 2019) by recomputing the radiation field doses on a phantom. For cohorts that include survivors of childhood cancers, phantoms should be scalable to the age or size of the patient at the time of RT.

For over two decades (>120 studies), the MD Anderson Late Effects Group has used an age-scalable computational phantom to reconstruct dose to organs throughout the body for large cohorts of childhood cancer survivors treated with conventional two-dimensional (2D) historic RT (Howell *et al* 2019). This phantom is currently coded in the FORTRAN 95 programming language and can only be used with co-planar beam geometries, which were standard in 2D planning. Furthermore, its current format does not support instantaneous or three-dimensional (3D) visualization. These limitations were acceptable for previous studies with cohorts treated with historic 2D RT. However, cancer survivors now include individuals treated with contemporary RT, e.g., 3D conformal RT, intensity- and volumetric-modulated RT, and particle therapy. For these individuals, complex treatment plans were designed using patients' computed tomography (CT) images within commercial treatment planning systems (TPS). Unlike in the 2D treatment planning era, dose to organs near the target volume are readily calculable as part of the treatment plans and therefore, will not need to be retrospectively recalculated. However, doses to distant organs will still need to be retrospectively reconstructed on computational phantoms, because CT images used for treatment planning may not be available for epidemiologic studies, and even if they are, the CT data will be limited to anatomy near the target volume and will not include distant structures that are typically of interest in such epidemiologic studies.

For retrospective whole-body dose reconstructions, the 'missing' anatomy could be supplemented by registering a patient's planning CT(s) with a computational phantom scaled to the age at RT. The MD Anderson Late Effects Group computational phantom is well suited for this purpose because (1) it is the most widely used phantom for late effects studies of historic RT and using this same phantom for studies involving contemporary RT will facilitate direct comparison of results between historic and modern studies; and (2) it can be uniquely scaled to any arbitrary age or height whereas other computational phantoms are limited to specific selected ages. However, the MD Anderson Late Effects Group computational phantom is programmed in FORTRAN language, which is not compatible for registration with patients' Digital Imaging and Communications in Medicine (DICOM) format CT images in commercial TPSs. Therefore, the primary objective of this study was to adapt the current model of our age-scalable computational phantom from the FORTRAN language to DICOM format for use within any commercial TPS, thereby facilitating epidemiologic studies of contemporary radiotherapy. Additionally, we report a detailed description of our age-based scaling functions, information that was not reported in our previous publications. Note that hereafter, we use phantom, FORTRAN, and DICOM for computational phantom, FORTRAN language, and DICOM format, respectively.

2. Methods

2.1 Phantom modeled in FORTRAN language (baseline phantom description)

The MD Anderson Late Effects Group phantom was previously described by Howell *et al* (2019) and Stovall *et al* (2006). The phantom was built by bounding the body regions, i.e., head, neck, trunk, arms, and legs, of a generic gender-neutral adult skeleton (age = 18 years)

by cuboids, which were then fit to a 3D grid of evenly spaced points (Figure 1). Each cuboid is defined by its eight corner points obtained from its fit to the 3D grid. Various organs are defined within the phantom's body regions as grids of points (Howell *et al* 2019).

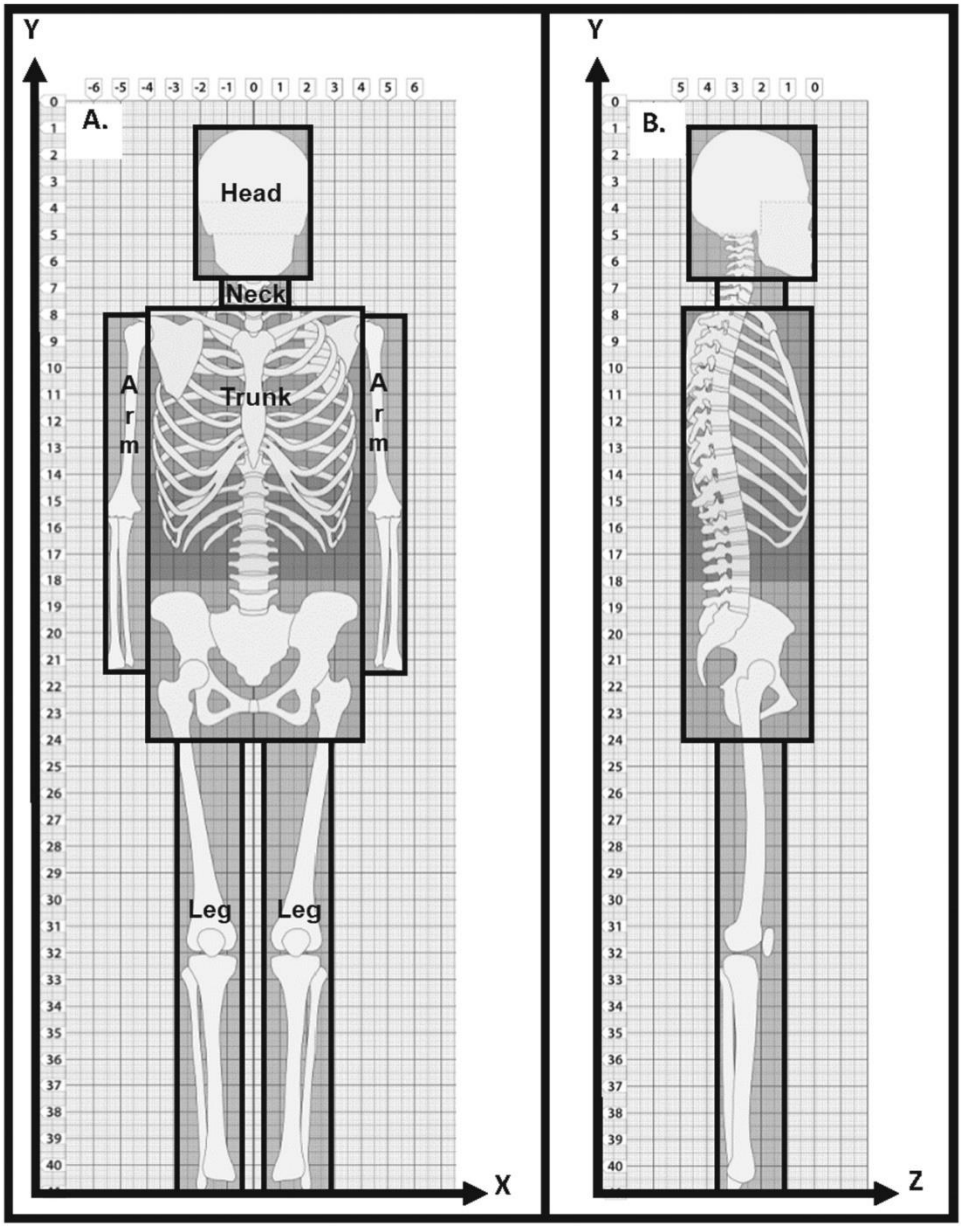

Figure 1: Diagrams of our computational phantom fitted to a 3D grid of points. (a) coronal view showing +x and –y axes and (b) sagittal view showing –y and –z axes. A skeleton is

overlaid on the phantom for anatomic reference. The scalable body regions (head, neck, trunk, and extremities) are delineated in frontal view.

2.2 Scaling functions

Because this phantom was intended for use in late effects studies of cancer survivors, including children, whose ages at the time of their RT ranged from infant to adult, it was necessary to define scaling functions to adapt the generic adult phantom (18 years of age) to any age. The head, neck, trunk, and extremities of the human body undergo non-uniform growth from infant to adulthood. For example, at birth the human head makes up approximately one quarter of the total height, but that proportion decreases to about one-seventh by adulthood (Huelke 1998). This non-uniform growth was quantitatively reported by the Society of Automotive Engineers based on measurements of 4127 US infants, children and youths through 18 years old (Snyder *et al* 1977). As a function of age, using these growth data, we plotted sizes of the head, neck, trunk, and extremities (legs and arms) in three dimensions (Figure 2). Then, we calculated the discrete scaling factor, $\mathrm{F_{dis}}$, by taking the ratio of the size of a specified body region r in a specified direction d at a given age a to its size in the generic phantom, equation (1).

$$\mathrm{F_{dis}(d, r, a)} = \frac{\mathrm{S(d, r, a)}}{\mathrm{S(d, r, g)}} \qquad \textbf{1}$$

where:

d ∈ {Left to right (x), superior to inferior (y), anterior to posterior (z)}

r ∈ {upper head (uh), lower head (lh), neck (n), trunk (tr), arms (ar), legs (lg)}

a ∈ {0.1 (1 month), 1, 3, 5, 10, 15, 18} and

g is a constant and is defined as age 18 years; the age of the generic phantom

Since equation (1) can only be used for scaling to discrete ages of 0.1 (1 month), 1, 3, 5, 10, 15, and 18 years, to allow scaling between these ages, we created age intervals of [0, 1), [1, 3), [3, 5), [5, 10), [10, 15), and [15, 18) and defined a continuous scaling function, for each age interval (equation (2)).

$$F_{cont}(d, r, a) = F_{dis}(d, r, a_{-}) + \frac{a - a_{-}}{a_{+} - a_{-}}\left(F_{dis}(d, r, a_{+}) - F_{dis}(d, r, a_{-})\right) \quad \textbf{2}$$

Where a_{-} and a_{+} are lower and upper age bounds, respectively. Each organ was considered to follow the same scaling as the body region in which it was located.

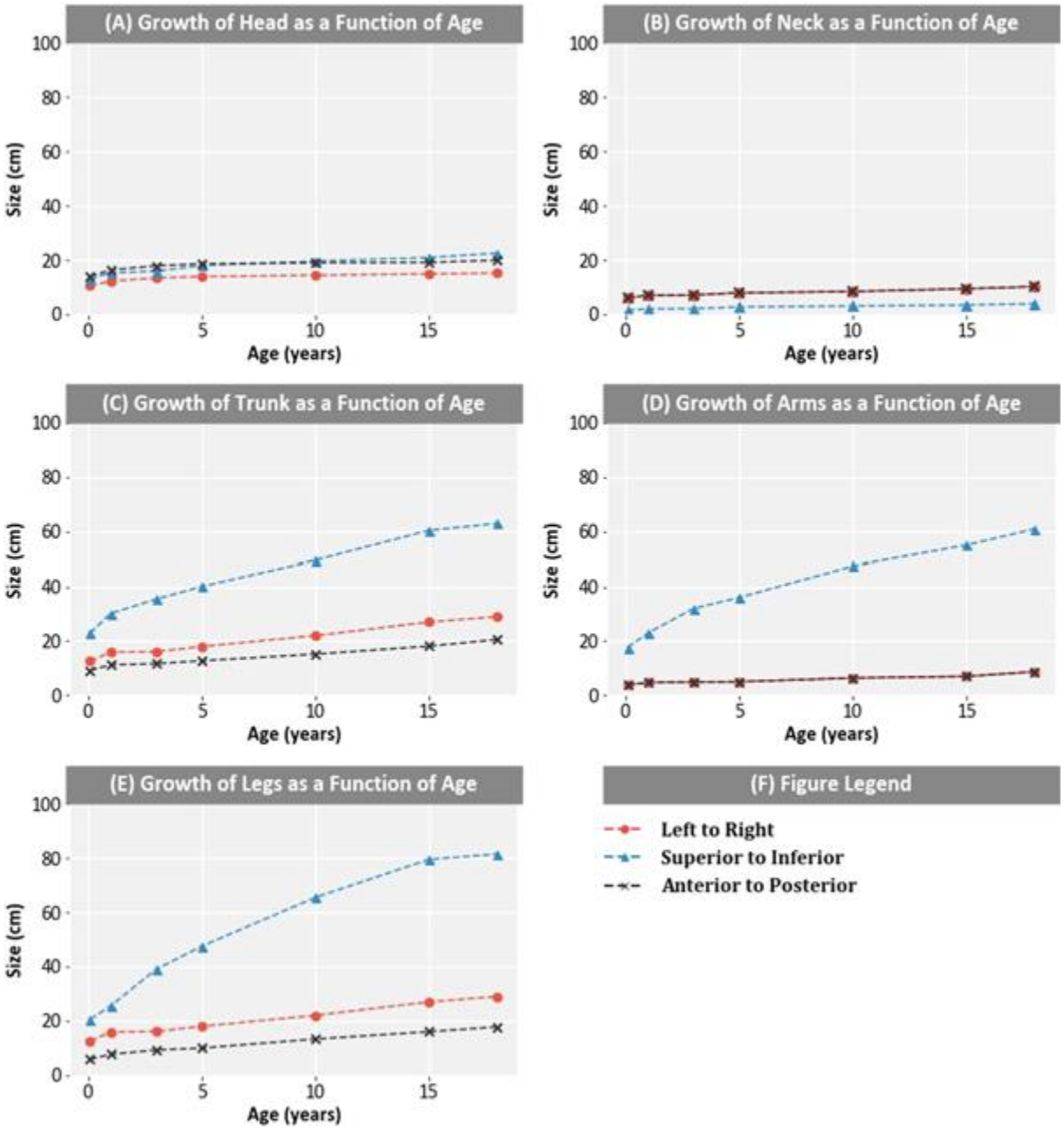

Figure 2: (A)–(E) Growth as a function of age from superior to inferior, left to right, and anterior to posterior for the head, neck, trunk, arms and legs for ages 1 month, 1, 3, 5, 10, 15, and 18 (adult) years (Snyder *et al* 1977, Huelke 1998).

2.3 Transformation functions

Each body region is represented by eight corner points and each organ is represented by a grid of points, where each point (P) is a set of three real numbers (coordinates) denoted by the variables x, y, and z, which represent the coordinates of a point. Once the necessary scaling factors are obtained using the scaling functions from section 2.2, we can apply these factors to each body region corner point and each organ point to transform them to various ages. Additionally, in the y and z directions, translations are also necessary so that all body regions remain contiguous and do not overlap as they scale; they are applied as described in the following paragraphs.

Since the generic phantom is symmetric about the x-axis (Figure 1), the transformed x-coordinate x_t can be obtained by taking the product of the continuous scaling factor (F_{cont}) and the x-coordinate (x), equation (3).

$$x_t = x \cdot F_{cont}(x, r, a) \quad \textbf{3}$$

Conversely, the generic phantom is asymmetric about the y-axis and starts at the $x - z$ plane where y = 1 cm (Figure 1). To obtain the transformed y-coordinate (y_t), we sum the product of the continuous scaling factor and the length for each body region ($l_{r,y}$) along the y-axis of the generic phantom, equation (4). The length of each body region along the y-axis is obtained by taking the difference between the inferior (ibr) and superior (sbr) boundaries of that body region in the generic phantom, i.e. y_{ibr_r}, and y_{sbr_r}, respectively. For the body region in which the point lies, the length is the difference between the y-coordinate (y) and the superior boundary of that body region.

$$\mathrm{y_t} = \sum_{\mathrm{r=uh}}^{\mathrm{r}} \mathrm{l_{r,y}} \cdot \mathrm{F_{cont}(y, r, a)} \text{ where } \mathrm{l_{r,y}} = \begin{cases} \mathrm{y - y_{sbr_r}}, & \mathrm{y} \in \mathrm{r} \\ \mathrm{y_{ibr_r} - y_{sbr_r}}, & \mathrm{y} \notin \mathrm{r} \end{cases} \quad \textbf{4}$$

Similarly, the generic phantom is asymmetric about the z-axis and the anterior aspect of each body region is at a different location in the x-y plane. Thus, to calculate a transformed z-coordinate (z_t) first we calculate the difference between the z-coordinate (z) and the anterior boundary of the body region in the z direction (z_{abr_r}). Next, we multiply this difference by the continuous scaling factor. Lastly, we add a (z_{shift}), equation (5).

$$z_t = \left(z - z_{abr_r}\right) \cdot F_{cont}(z, r, a) \; + \; z_{shift} \qquad \textbf{5}$$

where $\mathrm{z_{shift}}$ is described in equation (6) and differs according to the body region,

$$\mathrm{z_{shift}} \; = \; \frac{\mathrm{l_{r=head,z}} \cdot \mathrm{F_{cont}(z, uh, a)} - \mathrm{l_{r,z}} \cdot \mathrm{F_{cont}(z, r, a)}}{2} \qquad \textbf{6}$$

where $\mathrm{l_{r,z}}$ is the length of the body region in the z direction.

2.4 Phantom adaptation from FORTRAN to DICOM

For this study, we used RayStation V8.99 TPS (RaySearch Laboratories, Stockholm) because this TPS is used in our clinic and allows addition of user-specific customized features via Python scripting. We developed a script in Python that converts the generic phantom from FORTRAN to DICOM. The conversion is a 7-step process (Figure 3), which is executed through a graphical user interface (GUI) scripted within the RayStation TPS.

1. Import Data: The corner points of each body region and the points of 9 different organs for the generic phantom (age = 18 years) are imported from the FORTRAN code into RayStation. The organs that were modeled in this study are – Brain (Frontal Lobes (Right and Left), Temporal Lobe (Right and Left), Parietal Lobe (Right and Left), Cerebellum, Occipital Lobes, and Inner brain), Heart, Liver, Lungs (Right and Left), Stomach, Pancreas, Kidneys (Right and Left), and Thyroid Lobes (Right and Left).

2. Select Phantom Age: The user is then prompted to select the desired age. The user can select any value from 0.1 (i.e., newborn) to 18 years. Values are specified to the nearest tenth of a year. We assume growth stops at age 18 and for ages above 18, phantom is simply scaled to age 18.
3. Transform Coordinates: Equations (1) through (6) are hardcoded into the script. Based on the phantom age selected in step 2, each point imported from step 1 is transformed using equations (1) through (6). After this step, each organ and body region will have been scaled to the appropriate size based on the user-selected age.
4. Reorient Phantom: Since the coordinate systems are defined differently in the FORTRAN code and RayStation TPS, we apply an additional rigid transformation to reorient the phantom to the most common RT treatment orientation, which is head-first supine.
5. Convert Body Regions to DICOM format: Each body region is converted from a collection of vertices to a region of interest (ROI) using RayStation's Box ROI generation tool (through python script).
6. Convert Organs to DICOM format: Each organ is converted from a collection of grid points to an ROI using convex hull algorithm through python script.
7. Plot Phantom in RayStation: Once each body region and organ are in DICOM format, each can be plotted in RayStation.

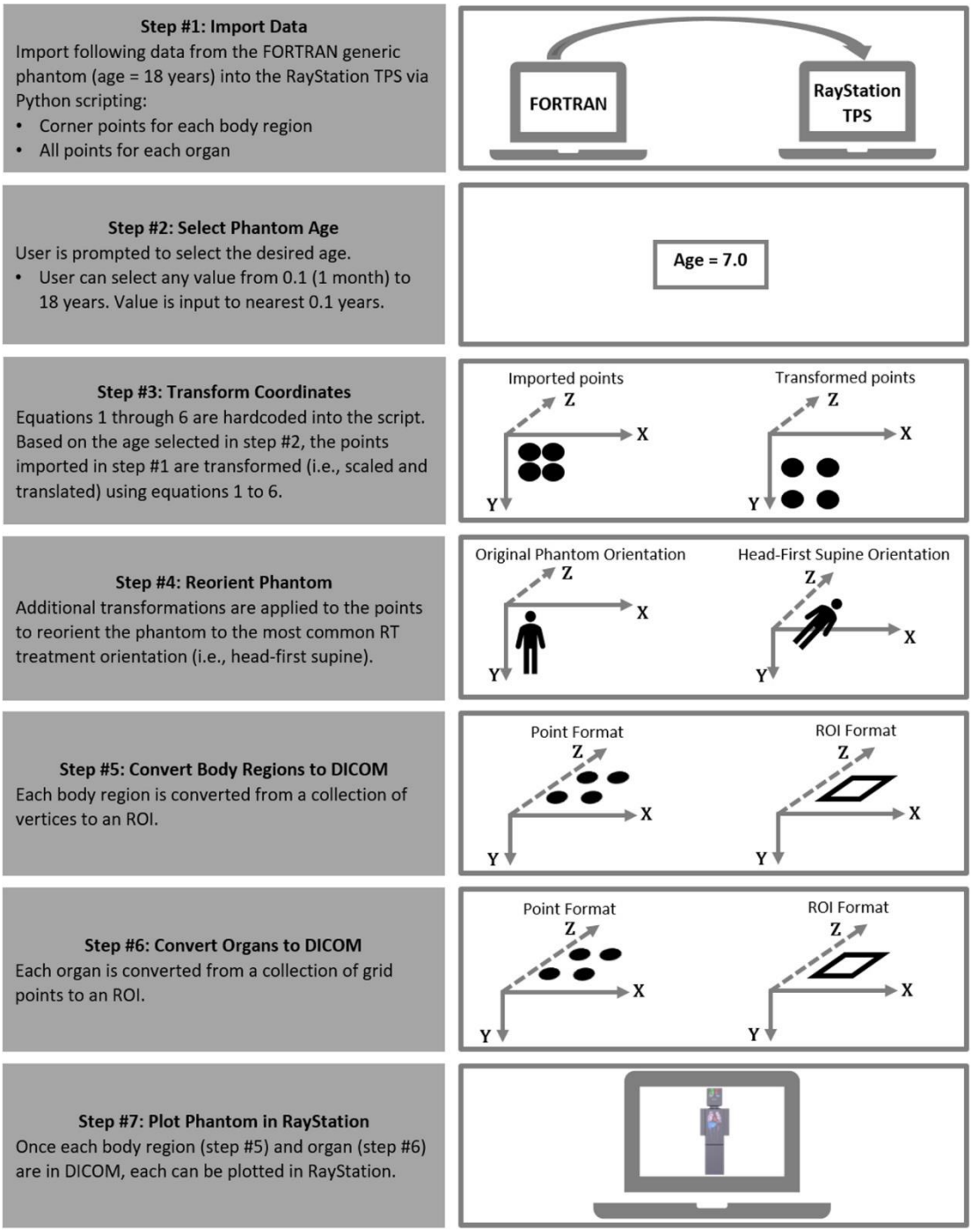

Figure 3: Flow chart explaining the adaptation of the phantom to DICOM format

Once the phantom has been generated in RayStation, users can export the phantom in DICOM format. This file can be uploaded into any DICOM-compatible TPS. A sample calculation of transformation of our generic 'adult' phantom to a 7-year-old phantom is

illustrated in the appendix A. Note that when we adapted our phantom from the FORTRAN to DICOM, we made two simplifications to the extremities: (1) the legs were simplified to consist of only one cuboid volume, as opposed to two separate cuboids and (2) the arm positions were constrained to a single position parallel to the sagittal plane (i.e. superior to inferior) as opposed to having variable positions of parallel or perpendicular to the sagittal plane of the body.

2.5 Validation

For this study, we performed two different validation approaches. For the first approach, we validated the conversion of our phantom model from FORTRAN to DICOM. To do this, we compared several geometric parameters between the phantom scaled to ages 1 month, 6 months, 1, 2, 3, 5, 8, 10, 15, and 18 years modeled in FORTRAN and DICOM. For the second approach, we compared the heights of the DICOM model of our phantom with population height data from the World Health Organization (WHO) and the Centers for Disease Control and Prevention (CDC) (Centers for Disease Control and Prevention 2000).

2.5.1 Comparison of FORTRAN phantom with DICOM phantom

The first metric we calculated was the percent difference. This metric was calculated for all corner points in each spatial dimension of each body region and for the volumes of each body region between the phantom modeled in FORTRAN and DICOM. For the locations of the corner points, we calculated this difference in the x-, y-, and z-coordinates individually for each age-scaled phantom. This analysis was done for the head, neck, and trunk body regions, which includes the majority of organs of interest for late effects studies. Percent differences (PD) were calculated as follows:

$$\mathrm{PD} = \frac{\mathrm{F} - \mathrm{D}}{\mathrm{F}} \times 100\% \quad (7)$$

where F corresponds to the coordinates (or volume) from FORTRAN (ground-truth) and D corresponds to the coordinates (or volume) from DICOM for the specified body region. The second metric we calculated was the normalized mean square distance (NMSD). The NMSD was calculated between the organs (heart, liver, lungs, stomach, and brain) for both phantoms using the following equation.

$$\mathrm{NMSD} = \frac{\sqrt{\sum_{\mathrm{i}}^{\mathrm{N}} (\mathrm{x_F} - \mathrm{x_D})^2 + (\mathrm{y_F} - \mathrm{y_D})^2 + (\mathrm{z_F} - \mathrm{z_D})^2}}{\mathrm{N}} \quad (8)$$

where, x, y, and z represent the coordinates of each organ point in the phantoms. The subscripts F and D represent that the coordinate of the point is from the FORTRAN and DICOM phantoms, respectively. N is the total number of points in each organ.

The third metric we calculated was the difference in heights between the FORTRAN and DICOM phantoms. This was calculated to ensure that the total height of the phantom was preserved when converted from FORTRAN to DICOM.

2.5.2 Comparison of DICOM phantom with WHO/CDC population height data

In order to determine if the heights of our age-scaled phantoms were consistent with the heights of children across the ages of infant to adolescent, we compared our age-scaled phantom heights with a reference dataset. Specifically, we compared our age-scaled DICOM phantoms with the 50th-percentile heights reported by the WHO for ages 1 month, 6 months, and 1 year old and with the averages of the 50th-percentile heights for males and females reported by the CDC for ages 2, 3, 5, 8, 10, 15, and 18 years.

2.6 Comparison with reference phantoms organ masses

In FORTRAN format, organs in our phantom were modeled as grids of points, making it impossible to compare organ volumes or masses with other reference phantoms. In the updated DICOM format, such comparisons are possible and therefore were performed as part of this work. Specifically, we compared organ masses of the DICOM phantom with reference masses from International Commission on Radiological Protection (ICRP) 89 (ICRP 2002) and University of Florida (UF)/National Cancer Institute (NCI) reference hybrid voxel phantoms for ages 6 days (newborn), 1, 5, 10, 15, and 18 years (Adult) (Lee *et al* 2010). We first calculated the organ masses for our DICOM phantoms (scaled to aforementioned ages) as a product of ICRU 46 reference densities and RayStation voxel-based volumes. The volume of the organs in our DICOM phantom is independent of sex but the ICRP 89 and UF/NCI reference phantoms provide sex dependent masses for the 15 years old and adult phantoms. In those cases, the average of male and female reference organ masses were calculated. Additionally, for the heart and stomach, the UF/NCI reference phantoms have masses for the wall and contents of these organs. For kidneys, the masses of the medulla, pelvis and cortex were reported individually. For heart, stomach and kidneys, we calculated the total mass by summing the mass of each organ's parts. Lastly, we computed the difference between the organ masses of the DICOM phantom and of the reference phantoms.

2.7 Dose calculation with DICOM phantom—Wilms' tumor example

To illustrate that our phantom can be used for dose calculations within a commercial TPS, we designed a treatment plan in RayStation and calculated dose to two organs at risk for our DICOM format phantom. The treatment plan was designed to be representative of a typical

RT plan for an individual in the Childhood Cancer Survivor Study (CCSS) cohort. To do this, we selected a common type of paediatric cancer, Wilms' tumor. We then performed a query of 7451 individuals in the CCSS expanded cohort (Leisenring *et al* 2009, Robison *et al* 2009) who received RT between 1985 and 1999 (data collected under IRB approved protocol and RT records previously abstracted). We identified 318 individuals diagnosed with Wilms' tumor who were treated with anterior-to-posterior and posterior-to-anterior (AP/PA) directed abdominal flank fields. From these 318 treatments, we selected the median treatment field parameters to simulate a typical (6 MV) right-sided flank field RT plan: [1] age at RT: 3.9 years (range 0.45–20.9 years), target dose 10.80 Gy (range 1.08–36.72 Gy), [3] superior field border: diaphragm (N = 203), [4] Inferior border: L5 (N = 139). The right-sided AP/PA treatment fields are illustrated for a 3.9-year-old phantom in FORTRAN and DICOM formats in Figure 4. Doses to two organs at risk—the liver and pancreas—were calculated. Specifically, we calculated the mean dose received by each organ and the percentage of each organ that received dose ≥ 5 Gy (V_5). For comparison, we simulated the same treatment for our FORTRAN format phantom and calculated liver and pancreas doses using our in-house calculation method.

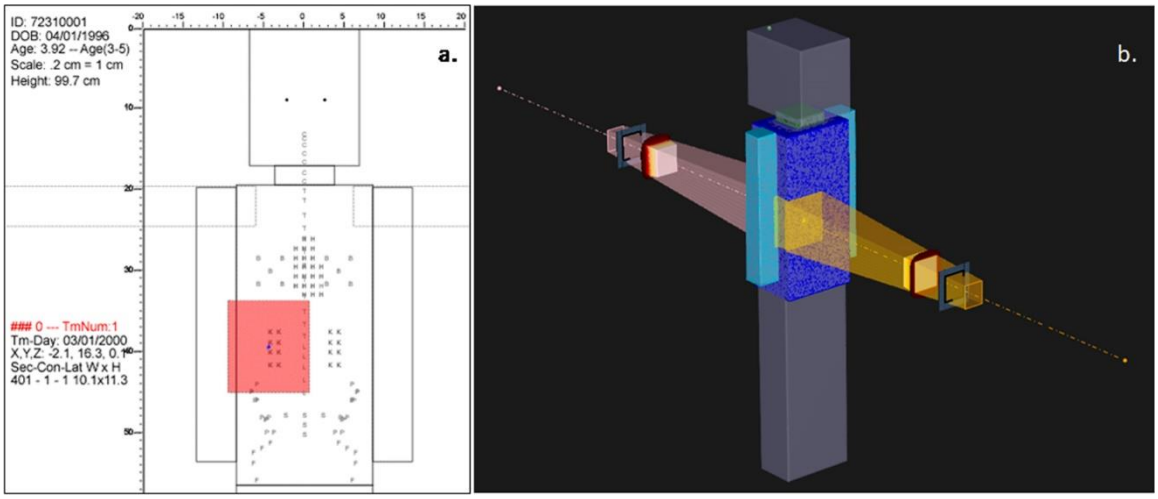

Figure 4: Right-sided AP/PA treatment fields simulated for Wilms' tumor RT plan on a phantom scaled to 3.9 years in (a) FORTRAN and (b) DICOM formats. The coordinates of the field isocenters and field borders were the same in both planning systems.

3. Results

3.1 Phantom modeled in DICOM standard

The age-scalable computational phantom modeled in DICOM format is illustrated in Figure 5, which includes 3D renderings of our phantom generated in RayStation TPS and scaled to ages 1, 5, 10, 15, and 18 (adult).

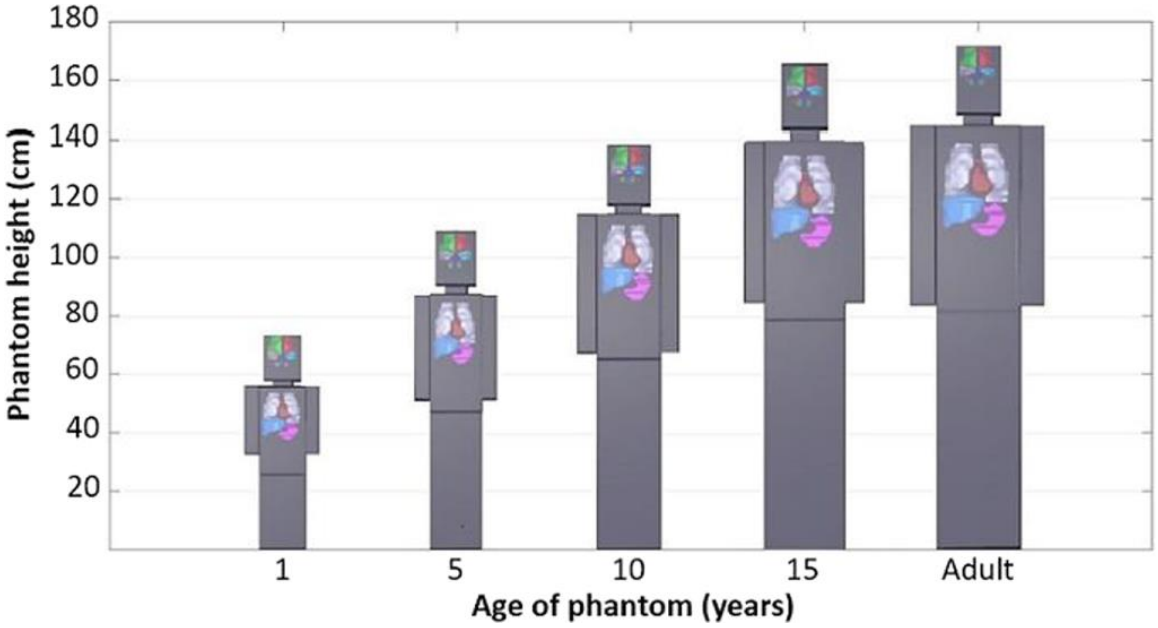

Figure 5: Illustration of TPS generated 3D renderings of age-scaled phantoms modeled in DICOM. Selected organs (brain, lungs, heart, liver, and stomach) were also rendered for each scaled phantom.

3.2 Comparison between phantom modeled in FORTRAN and DICOM

A histogram illustrating distribution and range of error in reproducing correct locations of body-region corner points is shown in Figure 6. All observed differences were within 3%, with 0% being most frequently observed. The results of the percent difference calculations in the volumes of the head, neck, and trunk of the two phantoms are shown in Table 1. For the volume analysis, we observed all differences within 3%.

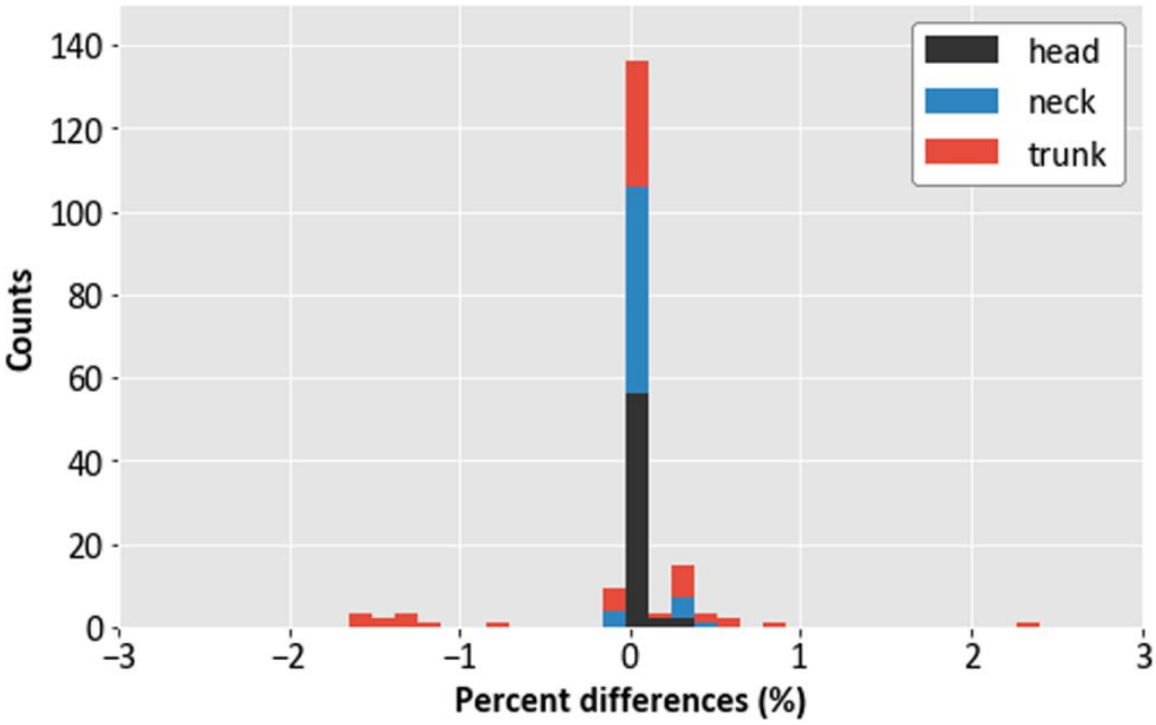

Figure 6: Histogram showing the frequency of percent differences in the corner points of body regions (excluding legs and arms) of the DICOM phantoms.

Table 1: Percent differences between the volumes of FORTRAN and DICOM phantom body regions

Body regions	Age (years)									
	0.1 (1 month)	0.5 (6 months)	1	2	3	5	8	10	15	18
Head	0.8	0.0	0.0	0.0	0.0	0.0	0.0	0.0	0.0	0.0
Neck	1.9	0.1	0.0	0.3	0.3	0.1	0.4	0.0	0.2	0.2
Trunk	2.8	1.2	1.3	1.2	1.3	1.3	1.3	1.3	1.2	1.2

The normalized mean square distance calculations resulted in strong agreement in the location of organs across the studied age range. The maximum NMSD was 7.80×10^{-2} mm for occipital lobe of age 1 month. When we compared the percent differences in the phantoms' heights modeled in DICOM and FORTRAN, we found accurate agreement

(difference = 0%) between the phantoms for ages 1, 3, 5, 10, and 15 years and a difference of 0.03% between the phantoms for age 18 years.

3.3 Comparison of DICOM phantom with population height data

Figure 7 shows, for ages 1 month through 20 years, a comparison of the heights of the age-scaled DICOM phantoms with the averages of the 50th-percentile CDC reported heights for males and females. The differences were 3.6, 2.1, 0.3, 1.4, 0.6, 1.0, and 0.7% for ages 2, 3, 5, 8, 10, 15, and 18 years, respectively. For 1 month, 6 months, and 1 year, the differences between the DICOM phantom heights and the WHO 50th-percentile heights were 6.9, 3.1, and 2.6%, respectively.

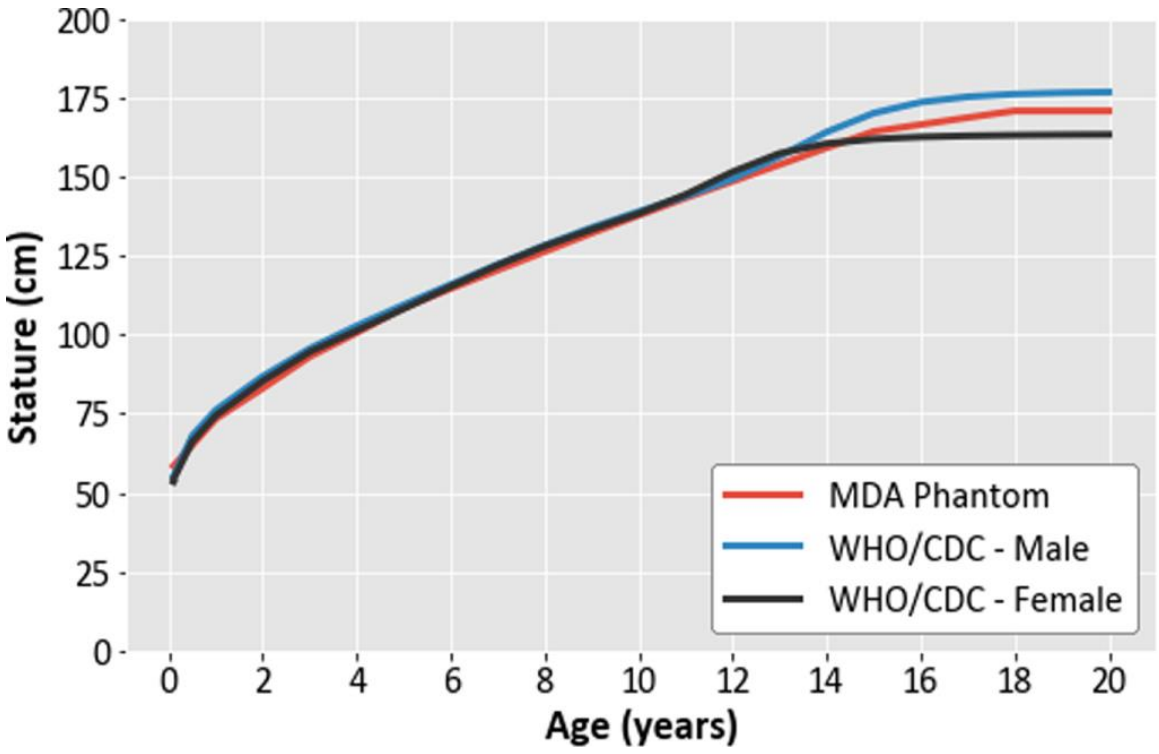

Figure 7: Comparison of the heights of the computational phantom modeled in DICOM with the WHO/CDC heights(Centers for Disease Control and Prevention 2000).

3.4 Comparison of organ masses of DICOM phantom with ICRP 89, and UF/NCI reference hybrid phantom data

The masses of nine organs from our DICOM phantom are listed in Table 2. Also reported in Table 2, are the absolute differences between organ masses in our phantom and those reported for ICRP 89 and UF/NCI phantoms. The differences are all negative (apart from newborn brain), i.e., the organ masses in both reference datasets are substantially greater than the organ masses in our phantom.

Table 2: Mass (in gram) of DICOM phantom organs and comparison with masses from ICRP 89 and UF/NCI reference hybrid voxel phantom data. In each case, the difference between DICOM phantom organ mass and ICRP 89 or UF/NCI reference masses were calculated

Organs	**Newborn**			**1 year**			**5 years**			**10 years**			**15 years**			**18 years (Adult)**		
	DICOM	DICOM - ICRP 89	DICOM- UF ref.	DICOM	DICOM - ICRP 89	DICOM - UF ref.	DICOM	DICOM - ICRP 89	DICOM- UF ref.	DICOM	DICOM - ICRP 89	DICOM –UF ref.	DICOM	DICOM - ICRP 89	DICOM - UF ref.	DICOM	DICOM - ICRP 89	DICOM - UF ref.
Heart	12.27	-33.73	-13.68	24.62	-73.38	-73.45	42.39	-177.61	-176.98	76.62	-293.38	-292.54	135.68	-464.32	-462.82	173.26	-556.74	-555.45
Brain	449.40	69.40	128.27	651.56	-298.44	-298.25	900.89	-344.11	-343.83	1003.63	-306.37	-305.84	1083.11	-276.89	-274.11	1153.46	-221.54	-215.17
Liver	54.32	-75.68	-75.36	108.86	-221.14	-220.61	181.62	-388.38	-383.20	318.69	-511.31	-510.14	572.21	-727.79	-726.37	738.61	-861.39	-858.70
Lungs	41.43	-18.57	-18.30	84.32	-65.68	-65.44	146.05	-153.95	-152.58	259.93	-240.07	-238.22	460.98	-364.02	-361.87	590.71	-484.29	-481.42
Stomach	25.27	-21.73	-7.05	48.26	-38.74	-38.41	75.79	-57.21	-56.59	133.35	-68.65	-67.44	225.17	-94.83	-94.01	287.68	-97.32	-97.14
Pancreas	3.13	-2.87	-2.86	5.03	-14.97	-14.90	7.28	-27.72	-27.67	11.56	-48.44	-48.37	20.56	-84.44	-84.19	26.31	-103.69	-103.26
Kidneys	2.76	-22.24	-23.48	5.05	-64.95	-68.31	9.21	-100.79	-105.85	16.22	-163.78	-172.78	27.62	-217.38	-229.23	34.17	-258.33	-272.23
Thyroid	0.26	-1.04	-1.03	0.44	-1.36	-1.35	0.60	-2.80	-2.80	0.55	-7.35	-7.35	0.61	-11.39	-11.31	0.62	-17.88	-17.82

3.5 Results from dose calculation (Wilms' tumor example)

The V_5 and mean dose (Gy) for liver and pancreas calculated with our in-house calculation system (with FORTRAN phantom) and the RayStation TPS (with DICOM phantom) are reported in Table 3; percent difference in each case is also reported. The percent differences between mean doses for liver and pancreas were −4% and 1%, respectively. The percent differences between V5 values for liver and pancreas were −6%and 7%, respectively.

Table 3: Percent difference between the V_5 and mean dose of DICOM and FORTRAN phantom organs

Organ at Risk	V_5 (%)			Mean Dose (Gy)		
	DICOM	FORTRAN	% Diff.	DICOM	FORTRAN	% Diff.
Liver	91%	96%	-6%	9.55	9.99	-4%
Pancreas	72%	67%	7%	7.57	7.50	1%

4. Discussion

In this study, we successfully adapted our phantom model from FORTRAN to DICOM, allowing for importation into any commercial TPS (RayStation, Eclipse, Pinnacle, Monaco, etc), where it can be used for a variety of dosimetry studies. Analogous to our FORTRAN phantom, our DICOM phantom can be scaled to any age and can be used to perform retrospective dose reconstructions for survivors treated with contemporary RT. In such studies doses to distant organs will need to be retrospectively reconstructed on computational phantoms because CT images used for treatment planning may not be available for epidemiologic studies, and even if they are, the CT data will be limited to anatomy near the target volume and will not include distant structures that are typically of interest in such epidemiologic studies. For example, for female pediatric brain cancer

survivors, whose CT scans only included the head and possibly the neck regions, organs of interest for late effects studies may include the heart, breasts, and ovaries, for which anatomical information is not present in the CT scan. In such cases, our phantom can be scaled to any age at RT and co-registered with the patient CT scan, and then doses to other organs can be reconstructed using the methodologies described in previous studies (Stovall *et al* 2006, Howell *et al* 2019). An important reason for using our phantom in late effect studies for cohorts treated with contemporary RT is to facilitate comparison with cohorts treated with historic RT. The dosimetry for RT-related late effects studies in the literature has been predominantly conducted using the MD Anderson Late Effects Group phantom. Howell *et al* (2019) reports more than one hundred late effects studies for which the MD Anderson Late Effects Group performed dose reconstructions for cohorts with thousands of childhood cancer survivor studies, e.g. the CCSS, St. Jude Lifetime (Hudson *et al* 2011, 2017), Adult Life after Childhood Cancer in Scandinavia (Asdahl *et al* 2015), and Dutch Childhood Oncology Group (Teepen *et al* 2017). Furthermore, other reference phantoms, e.g., UF/NCI, while anatomically more realistic compared to our phantom, are only available for discrete integer ages and cannot be scaled to any arbitrary age.

Our validation studies showed that our phantom was correctly adapted from FORTRAN to DICOM. The histogram analysis of the percent differences between the corner points of head, neck, and trunk body regions and volumes of the body regions were in good agreement (within 3%) and the majority (94.4%) of corner points agreed within 1%. The DICOM model of the phantom consists of organ contours developed from a grid of points that were obtained after transforming the points of the FORTRAN model of the phantom. The points defining the

organs were conserved quantitatively between the FORTRAN and DICOM models, with mean differences being less than 0.1 mm for all organ points. The maximum NMSD obtained was $7.80 \times 10^{-2} mm$ for occipital lobe of age 1 month. The heights of our age-scaled phantom agreed with WHO/CDC data within 7% from infant to adult, with best agreement for ages 5 years and older (<2%).

By modelling our phantom in DICOM, and, in particular, by converting our phantom's organs from grids of points to contours from which volume (and mass) could be derived, we were, for the first time, able to compare our phantom's organs masses with those from other reference phantoms. The results of this analysis demonstrated that the organ masses of our DICOM phantom are much less than those in both reference phantoms. The differences were similar in magnitude for comparisons with ICRP 89 and UF/NCI reference phantoms because the UF/NCI phantoms were adjusted to match ICRP 89 data (Lee *et al* 2010). It was not unexpected that our organ masses would differ from more recently developed ICRP 89 and UF/NCI phantoms because the organs in our FORTRAN phantom, which were the basis of the organs in the DICOM phantom, were developed from crude sampling of organ points from cross-sectional anatomical images (Howell *et al* 2019). While the differences in mass were large, it is important to underscore that dosimetry conducted with our in-house dose calculation methodology and FORTRAN phantom did not use organ masses for calculations. In that system, we calculated doses to the individual points comprising an organ. Then from those data, the mean organ doses were taken as the mathematical average of the point doses. Similarly, dose-volume metrics were approximated from percentage of points, e.g., the V_5 was estimated from the percentage of points with dose ≥5 Gy.

In this study, we also illustrated that our phantom can be used for dose calculations within a commercial TPS. This example calculation demonstrated that our DICOM phantom can be scaled to any age (here 3.9 years), not just the ages illustrated in Figure 1. Also, by selecting an example case that was typical of the types of calculations for which our in-house calculation method has been used, we were able to perform the same calculation for both the FORTRAN and DICOM format phantoms for direct comparison. Notably, we observed reasonably good agreement (within 7%) between the two calculation methods with the FORTRAN and DICOM phantoms (Table 3). We attribute the differences between doses to the more accurate collapsed cone dose calculation algorithm in the RayStation TPS compared to the very simple 2D method used in our in-house calculation system.

While the DICOM model of our phantom was validated and can be used for dose calculations in a commercial TPS, the comparison of organ masses for our DICOM phantom and the organ masses from the reference phantoms revealed that our organs are too small and highlighted that refinement is necessary. The enhancement that we accomplished in this study, converting our phantom from FORTRAN to DICOM format, opens new avenues to achieve this. Namely, we can now register the DICOM model of our phantom with patients' and other phantoms' (Lee *et al* 2010) CT images to evaluate the correspondence of organs.

Phantoms enhancements that we are working towards include, redefining organs to be more anatomically realistic in size and shape and adding substructures to more organs. For example, the heart, an important organ for RT-related late cardiac disease, was developed using an anatomy atlas and was modeled as a 55 point grid with no substructures. We can enhance the shape and size of the heart based on the realistic anatomy and compare the new

model with models from UF/NCI reference phantoms. The heart model in our phantom could be further refined by adding substructures and increasing the resolution of points that would enable calculations of RT doses to specific substructures. These substructure doses could be used to further enhance dose-response models for RT-related late cardiac disease, which at present are based on whole-heart doses (Mulrooney *et al* 2009, Haddy *et al* 2016, Bates *et al* 2019). Additionally, other organs in the FORTRAN phantom were designed with low resolution, e.g., kidneys and pituitary glands have 15 and 1 points, respectively. For these low-resolution organs, we were not able to create contoured volumes that can structurally represent the organ in the RayStation TPS. Finally, we are presently working on adding a colorectal model to our phantom to understand the relationship between dose to the colon/rectum (and its substructures) and treatment-related colorectal second cancers in childhood cancer survivors. Existing studies on this topic have not included detailed colorectal dosimetry (Henderson *et al* 2012, Nottage *et al* 2012, Tukenova *et al* 2012).

5. Conclusion

We successfully adapted our age-scalable computational phantom from the FORTAN language to DICOM format, which can be imported into any commercial TPS. The modelling of the phantom in DICOM allows visualization of organs and body regions in three dimensions, which was not done before. Most importantly, the phantom modeled in DICOM can be used for late effects studies of cohorts that include survivors treated with contemporary RT.

Chapter 4: Scaling of Whole-Body Computed Tomography-Based Anatomy to Any Age

This chapter is based on the following manuscript which was submitted to Biomedical Physics & Engineering Express Journal, and it is under review.

A.C. Gupta, C.A. Owens, S. Shrestha, C. Lee, S.A. Smith, R.E. Weathers, T. Netherton, P.A. Balter, S.F. Kry, D.S. Followill, K.T. Griffin, J.P. Long, G.T. Armstrong, R.M. Howell, "Implementation and Validation of Non-Uniform Body Region Specific 3D Age-Scaling Functions to Scale Whole-Body Computed Tomography Anatomy to Any Arbitrary Age for Late-Effects Studies of Childhood Cancer Survivors," In Review (2021).

This chapter describes the results of Specific Aim 2: Apply ASFs to scale the whole-body CT based anatomy to any arbitrary ages, and validate scaling with ground-truth anatomy and reference data.

1. Introduction

In the decades after treatment, childhood cancer survivors are at high risk for developing treatment-related late effects due to high survival rates for pediatric cancers (> 84%) and long-life expectancy (Travis and Boice 2012, Armstrong *et al.* 2016, Gibson *et al.* 2018). Radiation epidemiologic studies of childhood cancer survivors seek to establish dose-response relationships between specific late effects and the dose from radiotherapy (RT) to the organ in which the late effect occurred (Travis *et al* 2011). Most childhood cancer survivor cohorts include survivors treated in the pre-computed tomography (CT) era of RT and organ doses must, therefore, be estimated by reconstructing RT treatment fields on

surrogate anatomy. The most used surrogate anatomy for retrospective RT reconstruction is computational phantoms.

In the last 50 years, computational phantoms have experienced dramatic advancements, beginning with the ICRU spherical models (ICRU 1992a) and simple first-generation stylized phantoms at discrete ages (ORNL 1966) to the advanced age-scalable computational phantoms (Howell *et al* 2019) and to the highly realistic patient-dependent hybrid computational phantom libraries (Lee *et al* 2010, Segars *et al* 2010, Zaidi and Tsui 2009, Xu 2014). Taking advantage of the modeling flexibility, the reference size hybrid phantoms were modified into body size-dependent phantoms such as the phantom library developed by the University of Florida and National Cancer Institute (UF/NCI) consisting of 158 pediatric phantoms of various heights and weights (Geyer *et al* 2014). When using such phantom library to retrospectively reconstruct RT treatment of a childhood cancer survivor with no CT images, a phantom of nearest height and/or weight of the survivor can be selected as a surrogate. This approach is only feasible when both the height and weight of a survivor are known (Kalapurakal *et al* 2018), which, however, is not always the case in historic RT records. Therefore, the age at RT is commonly used as a surrogate for height and weight where reference size phantoms are adopted. Since the reference size phantoms are usually available at discrete ages (e.g. newborn, 1, 5, 10, 15, and adult), the nearest available discrete age would be selected for RT reconstruction for a survivor. For example, the 5-year-old reference size phantom would be selected for a survivor that was 3.9-year-old at the time of RT treatment. This age discrepancy, further increases uncertainty in dose reconstruction as the organ size of a 3.9-year-old survivor would be smaller than that of a standard 5-year-old

phantom which, (1) for partially in-beam organs, would result in a larger fraction of the organs being in-beam, overestimating dose and (2) for out-of-beam organs, would result in organs being farther from the field, underestimating organ dose. Dosimetric uncertainties can translate to uncertainties in risk estimation, which in some instances can be as much as 70% (Vũ Bezin *et al* 2017).

Since age is generally the only height and weight surrogate available in historic RT records, age-based scaling of computational phantoms is frequently used in RT epidemiology studies. The MD Anderson Late Effects Group developed and validated a computational phantom (used in over 120 radiation epidemiology studies) that can be scaled to any ages from infant to adult (Stovall *et al* 2006, Howell *et al* 2019) based on age-scaling functions (ASF) that were developed from growth data of 4,127 U.S. infants, children, and youths through 18 years of age (Snyder *et al* 1977). This capability is compatible with what is typically available in historic RT records and also allows for the scaling of the computational phantom to the exact age of the survivor at the time of RT treatment. Recently, the MD Anderson phantom and the ASFs were implemented and validated in the Digital Imaging and Communication in Medicine (DICOM) standard (Gupta *et al* 2020). This adaptation makes it possible to use ASFs to scale other DICOM-formatted phantoms. The main purposes of this investigation were to (1) conduct a feasibility study to scale reference size discrete age phantoms from the UF/NCI phantom library to both discrete and continuous valued ages that are common in RT epidemiologic studies of childhood cancer survivors and (2) to evaluate the dosimetric impact of using exact age-scaled phantoms as opposed to nearest-age matched

phantoms. Hereafter, we have interchangeably used discrete aged phantoms to represent reference size UF/NCI phantoms.

2. Methods

2.1 The University of Florida/National Cancer Institute (UF/NCI) computational phantom library

We adopted the UF/NCI computational phantoms to test our age-scaling methods. The phantom library consists of two groups: the reference size phantoms and the body size-dependent phantoms. The reference size phantom library was developed from the manual segmentations of high-resolution CT scans of cadavers and patients at different discrete ages from 6 days to 25 years (Lee *et al* 2010). The phantoms were originally scaled to match the 50^{th} percentile heights, arm lengths, acromial breadth, and body region circumference from several reference datasets as reported in Lee *et al* (2010) and Johnson *et al* (2009). The organ volumes were represented by a single volume which precluded its comparison with the International Commission on Radiological Protection Publication (ICRP) 89 data as autopsy data are mostly reported in terms of wall and internal contents of the organs. Therefore, the single organ volumes were later separated into organ wall, tissue, blood, and air for discrete aged phantoms. Furthermore, skeleton, muscles, lymph nodes, and blood vessels were added to make the phantom more anatomically realistic. With the incorporation of updated organs and additional structures at discrete ages, the ICRP adopted the UF/NCI pediatric male and female phantoms (age: 6 days, 1, 5, 10, and 15 years) in ICRP 143 report (Bolch *et al* 2020). Later, the heights of the phantoms were up-/down-scaled and the circumference of the body

regions was modified (by adding fat layer) to create a library of 158 pediatric and 193 adult phantoms of varying heights and weights i.e. body-mass index (BMI) (Geyer *et al* 2014). These phantoms were later converted to DICOM-RT format, with accompanying CT images and segmented organ structures, using the DICOM-RT Generator developed in Griffin *et al* (2019).

For our feasibility study, we used reference size male and female UF/NCI phantoms at ages 1, 5, 10, 15, and 35 years as this phantom set allows us to validate our age scaling methodologies at discrete ages and also allows us to scale the phantoms to any continuous-valued ages that are common in RT epidemiological studies of pediatric survivors. We excluded the newborn phantoms because the neck is flexed in these phantoms, which results in an inherent error due to the difference in neck orientation; we are only interested in scaling errors from our ASFs.

For our dosimetric assessment, we obtained one reference size 5-year-old UF/NCI phantom and seventeen body-size dependent phantoms that were created from the reference 5-year-old phantoms. We selected the age of 5 years in our study because this is the closest age to the median age of Childhood Cancer Survivor Study (CCSS) cohort (Leisenring *et al* 2009, Robison *et al* 2009) which is adopted in this study to obtain continuous valued-ages that are common in RT epidemiologic studies (as described in detail in section 2.4). The age, number, height, and weight of the phantoms used in this study are shown in Table 4.

Table 4: Parameters of UF/NCI phantoms selected in this study

Age (years)	Number of phantoms		Heights (cm)*		Weight (kg)		Type
	M	F	M	F	M	F	
Phantoms used in the feasibility study							
1	1	1	76.4	76.4	10	10	Reference
5	1	1	110.3	110.3	19	19	Reference
10	1	1	139.9	139.9	32	32	Reference
15	1	1	169.9	161.9	56	53	Reference
Adult (35)	1	1	174.8	163.6	73	60	Reference
Phantoms used in dosimetric assessment studies							
5	9	8	95.3-115.5	95.3-115.5	15-30	15-30	Body-size dependent

*Heights were measured from DICOM file. M= male and F=female

2.2 Modification of MD Anderson Late Effects Group scaling methodologies for UF/NCI phantoms

2.2.1 Original MD Anderson Late Effects Group scaling methodologies

Our baseline 3D phantom (hereafter called the generic phantom) consists of body regions that define the head, neck, trunk, legs, and arms, and 25 organs (Stovall *et al* 2006, Howell *et al* 2019). Phantom scaling methods are described in detail in Gupta *et al* (2020) and will be summarized here. The generic phantom is scaled by body region and direction-specific ASFs, which account for non-uniform growth of the generic phantom to any arbitrary age in right-left (RL) or x, anterior-posterior (AP) or y, and inferior-superior (IS) or z directions. Since the ASFs are body region-specific, the organs located within each body region are scaled with the same ASFs as the body region. The ASFs have two components and hence, scaling is executed in two - steps. In the first step, the body region and direction-specific scaling factors are determined based on the target age. For the ages $a \in \{0.1, 1, 3, 5, 10, 15, 18$ years$\}$, we use discrete scaling functions, F_{dis}, which was originally estimated from 50th percentile body

measurements reported by Snyder *et al* (1977). For any other ages, we perform linear interpolation in between closest discrete ages to estimate the continuous valued age scaling function, $\mathrm{F_{cont}}$. In the second step, $\mathrm{F_{dis}}$ or $\mathrm{F_{cont}}$ are incorporated in the body region and direction-specific transformation equations which transform the 3D points with respect to the reference lines and boundaries of body regions. For example, in the RL directions, points were transformed about x=0, and in the AP direction, points were transformed with respect to the anterior boundary of the body regions. This enables accurate scaling and localization of the 3D points of each body region and organ. Lastly, since the body regions and organs are in point format, the points for each structure are converted to surface contours using convex hull algorithms.

2.2.2 Modifications in scaling factor estimation

Since the UF/NCI phantoms are available at discrete ages, we developed a protocol to apply our ASFs to scale the UF/NCI phantoms from discrete ages to our generic phantom dimensions and then scale from the generic phantom dimensions to any arbitrary age. Therefore, the scaling function, $\mathrm{F_{a\rightarrow a_t}}$, in a head-first-supine orientation, is obtained by taking the ratio of scaling functions $\mathrm{F_{dis}}$ or $\mathrm{F_{cont}}$ of a specified body region, r, in a direction, d, at an arbitrary target age, $\mathrm{a_t}$, and $\mathrm{F_{dis}}$ of the same r in the same direction but at the original discrete age, a, as shown in equation (9).

$$\mathrm{F_{a\rightarrow a_t}(d,r,a)} = \frac{\mathrm{F_{dis\ or\ cont}\ (d,r,a_t)}}{\mathrm{F_{dis}(d,r,a)}} = \begin{bmatrix} \mathrm{F_x} \\ \mathrm{F_y} \\ \mathrm{F_z} \end{bmatrix} \qquad \textbf{9}$$

where:

$\mathrm{d} \in$ {left to right (x), anterior to posterior (y), and inferior to superior (z)}

$r \in$ {head (h), neck (n), trunk (tr), arms (ar), legs (lg)}

$a \in$ {0.1 (1 month), 1, 3, 5, 10, 15, 18}, and

a_t lies in the age intervals {[0, 1), [1, 3), [3, 5), [5, 10), [10, 15) and [15, 18)}

F_x, F_y and F_z are the scaling factors and are represented in the matrix form.

2.2.3 Modification in transformation equations

Two factors drive the modification of our original transformation equation: the availability of the UF/NCI phantom in DICOM format and adoption of the RayStation treatment planning system (TPS), which is currently used in our clinic. The body regions and organs of the UF/NCI phantom are in 3D region of interest (ROI) format in RayStation and the TPS has the "TransformROI3D" function where scaling, rotation, and translation factors are entered in the 4x4 transformation matrix $\mathbf{T}$ as shown in equation (10). Since the transformation that is performed in RayStation only involves scaling and translation, all the rotational components are equal to zero.

$$\mathbf{T} = \begin{bmatrix} F_x & 0 & 0 & t_x \\ 0 & F_y & 0 & t_y \\ 0 & 0 & F_z & t_z \\ 0 & 0 & 0 & 1 \end{bmatrix} \quad \textbf{10}$$

Where, $F_x, F_y, \text{and } F_z$ are the scaling factors (from equation (1)) that scale an ROI in the RL, AP, and IS directions, respectively. t_x, t_y and t_z translate an ROI in the RL, AP, and IS directions, respectively.

To adapt our original transformation equations (Gupta *et al* 2020) correctly in the "TransformROI3D" function, we modified our original approach which we will summarize here. We first performed scaling of ROIs using scaling matrix $\mathbf{T_s}$ (equation (11)) where

rotational and translational elements are zero. We then translated the scaled ROI using $\mathbf{T_t}$ (equation (12)) where scaling and rotational elements are zero. Equations (11) and (12) are the derivatives of equation (10).

$$\mathbf{T_s} = \begin{bmatrix} F_x & 0 & 0 & 0 \\ 0 & F_y & 0 & 0 \\ 0 & 0 & F_z & 0 \\ 0 & 0 & 0 & 1 \end{bmatrix} \quad \textbf{11}$$

$$\mathbf{T_t} = \begin{bmatrix} 1 & 0 & 0 & t_x \\ 0 & 1 & 0 & t_y \\ 0 & 0 & 1 & t_z \\ 0 & 0 & 0 & 1 \end{bmatrix} \quad \textbf{12}$$

If R(x,y,z) is the unscaled 3D ROI that spans the patient in the RL, AP, and IS directions, then the scaled ROI $R_T(x, y, z)$ at an arbitrary age a_t is obtained by

$$R_T(x, y, z) = \mathbf{T_s} \cdot R(x, y, z) \quad \textbf{13}$$

The above operation results in displacements in the centroids of the body regions and organs as each body region and its corresponding organs undergo non-uniform scaling. To remedy this, we first correct the centroids of the body region and then the centroids of the organs (also presented in Figure 8). For body regions, we first determine the centroid of the scaled head ROI. Then, we translate it back to centroid before scaling. We then translate all other scaled body regions to the mid-plane (in AP and RL directions) of the scaled head ROI using $\mathbf{T_t}$. The translations in IS direction, for correct body region stacking, is determined by scaling the distance between the centroids of unscaled head and body regions ROI as described in more detail in Gupta *et al* (2020). Organs ROI are translated with respect to centroids and the anterior and upper boundary of the body region they belong to. This results in the

accurate scaling of the original depth of organs in all directions. Therefore, the centroids $(X_{c_t}(o), Y_{c_t}(o), Z_{c_t}(o))$ of the scaled organ ROI, o, are given by:

$$X_{c_t}(o) = X_{c_t}(r) \pm \text{abs}[X_c(o) - X_c(r)] \cdot F_{a_{\rightarrow}a_t}(x, r, a) \quad \textbf{14}$$

$$Y_{c_t}(o) = Y_{abr_t}(r) + \text{abs}[Y_c(o) - Y_{abr}(r)] \cdot F_{a_{\rightarrow}a_t}(y, r, a) \quad \textbf{15}$$

$$Z_{c_t}(o) = Z_{ubr_t}(r) - \text{abs}[Z_c(o) - Z_{ubr}(r)] \cdot F_{a_{\rightarrow}a_t}(z, r, a) \quad \textbf{16}$$

Where,

$X_{c_t}(r)$ and $X_c(r)$ are the centroids of the scaled and unscaled body region, r, in the RL direction, respectively. The + and – signs accounts for the organs located in the right and left directions, respectively, from the mid-plane of the patient

$X_c(o), Y_c(o)$ and $Z_c(o)$ are the centroids of unscaled organ, o, in the RL, AP, and IS directions

$Z_{ubr_t}(r)$ and $Z_{ubr}(r)$ are the upper boundaries of scaled and unscaled body regions, r, in the IS direction.

Once $(X_{c_t}(o), Y_{c_t}(o), Z_{c_t}(o))$ is calculated, the organ ROIs are translated to their correct centroid using $\mathbf{T_t}$.

Although UF/NCI phantoms were used in this study, the above methodologies can be applied to any DICOM-compatible phantom or whole-body patient anatomy for which ROI of the body regions and organs of interest are available.

2.3 Scaling of computational phantoms to arbitrary ages

To perform the scaling and generating of DICOM files of the scaled phantoms, DICOM files of the original phantoms are imported into the RayStation v10B TPS. We developed Python scripts that can scale any whole-body CT-based anatomy from one age to another as long as we have organ contours/ROI or points representing the ROI. This task is accomplished with three different in-house Python scripts using the following steps. A general overview of the steps for downscaling a 5-year-old to a 3.9-year-old is presented in Figure **Error! Reference source not found.**8.

1. **Data preparation:** The current and target ages of the phantom or patient anatomy are entered in the Python script. A quality check is performed to ensure that the phantom is in head-first-supine orientation and the names of all organs within the phantom match a name from the list of names that are defined in the script.
2. **Body region separation**: Since the UF/NCI phantom does not have the body regions defined, we divided the whole-body ROI into head, neck, trunk, arms, and legs based on standard bony landmark measurements performed on the phantom. For example, the boundary of the head and neck is at the intersection of the 2^{nd} and 3^{rd} cervical vertebrae. The separation was performed using ROI algebra in the RayStation TPS.
3. **Localization of organ centroids:** Distances between the organ centroids and the boundary of body regions are calculated. In the RL, AP and IS directions, the distance is calculated with respect to the midline of the patient, the frontal boundary of the cuboid enclosing the body regions, and the upper boundary of the cuboid enclosing the body regions. The calculated distances are scaled using equation (9).

4. **Scaling and translation of body regions and organs:** Using equations (9) and (13), each body region is scaled and translated per the description in section 2.2.3. The organs are also scaled using equations (9) and (13) and are translated using equations (14)-(16)
5. **Post-processing:** The boundaries of body regions in the IS direction are checked for gaps or any unanticipated translation. The manual translation is performed for such cases. Steps 2 through 4 involve multiple ROI algebra operations, which could result in small holes in the contours, contour overlaps, and fragments. This is fixed by using the "Simplify contours" function in RayStation.
6. **Assignment of Hounsfield unit (HU) values:** Once the phantoms are scaled in the TPS, the size of the body regions/organs changes in each slice, and as a result, the contour/ROI boundaries do not cover the same voxels of the CT scan. Because of this, the HU values originally assigned to each voxel no longer represent the scaled anatomy. To assign the correct HU values to each voxel, the DICOM files are exported and are processed with our Python script. The following lists the sub-steps within step 6.
    a. Using the polygon function of the skimage.draw Python module (Van Der Walt *et al* 2014), we trace the boundary of contours on the slices of CT scan. Using the traced boundary, we create masks on each slice and then we record the voxel locations.
    b. For discrete ages, we obtain HU values from the DICOM RT generator software (Griffin *et al* 2019). For continuous-valued age, we perform linear interpolation to estimate the HU values.

c. For each scaled organ ROI, we assign same HU values to each voxel that reside within the ROI boundary.

The result of step 6 is a CT scan with voxels that are assigned HU values based on the ROI boundary that a voxel resides in.

7. **Quality Check:** DICOM files are imported into RayStation TPS and are visually inspected by the user for artifacts and discontinuity of the voxel HU values at ROI boundaries. Contours are simplified and holes are removed. Afterward, the DICOM files are ready for the dose calculations.

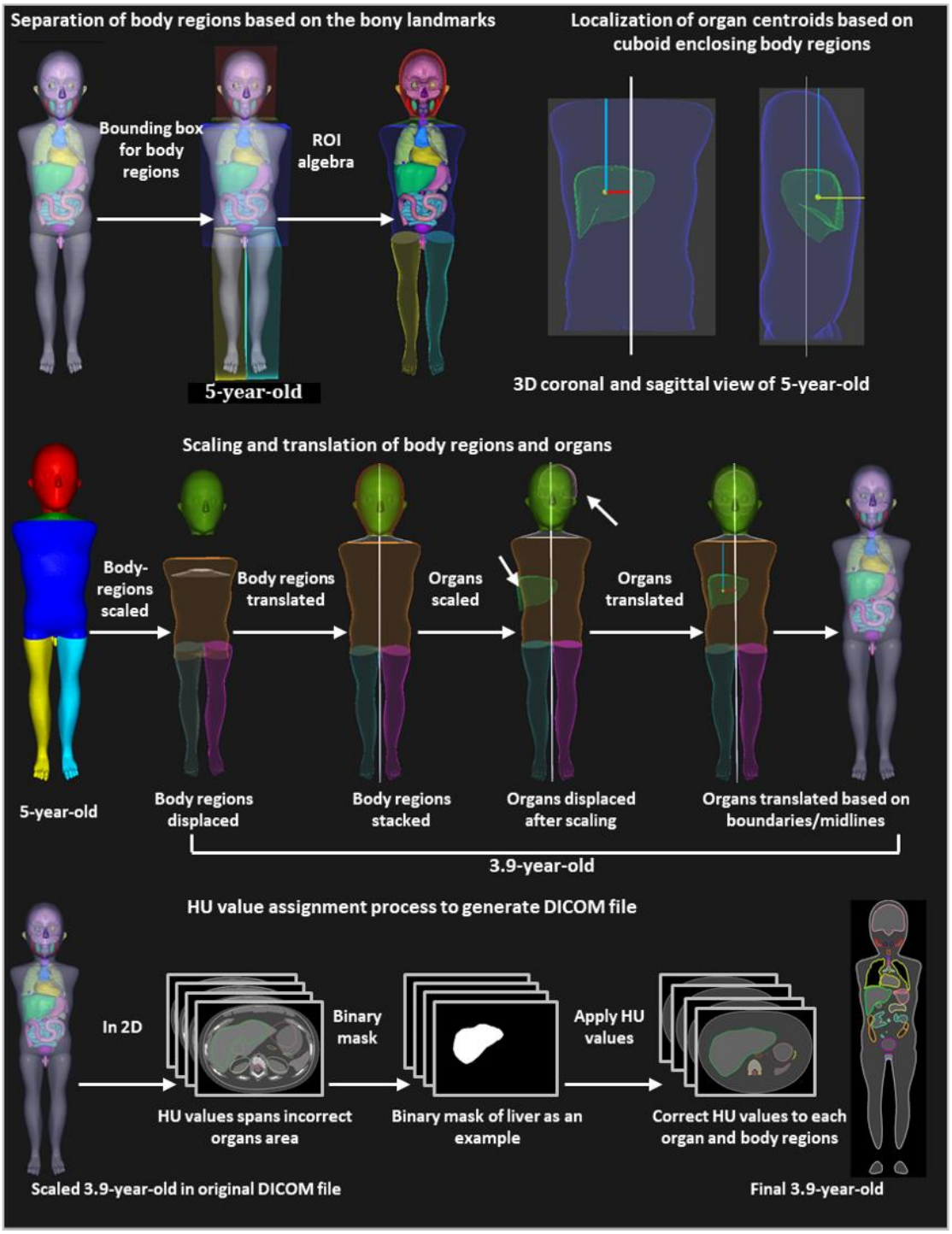

Figure 8: Steps used in the scaling process of the UF/NCI phantoms to arbitrary ages. Scaling of a reference size 5-year-old to 3.9-year-old is shown as an example.

2.4 Feasibility and validation study

For the feasibility study using our ASFs, we downscaled both male and female discrete-aged phantoms (5, 10, 15 and 35 years) to the nearest lower discrete ages (1, 5, 10 and 15 years), resulting in 8 scaled phantoms (4 male and 4 female), and validated the scaled phantoms with the original UF/NCI phantoms available at that age, i.e., ground-truth phantoms. For example, the 5-year-old male phantom was scaled to the size of a 1-year-old phantom and was validated with a ground-truth 1-year-old male phantom. To show the feasibility of scaling discrete-aged phantoms to continuous valued-aged phantoms, we downscaled the nearest age-matched discrete-aged phantoms to three different ages, representative of the CCSS expanded cohort. Specifically, both male and female 5-year-old phantoms were downscaled from reference size UF/NCI phantom library to 3.9-year-old phantoms (median age at RT for Wilms' tumor patients in CCSS expanded cohort). Similarly, both male and female 10-year-old phantoms were downscaled to 8.1 and 9.0-year-old phantoms (median ages at RT for craniospinal tumor patients and for entire CCSS expanded cohort, respectively). A total of 14 phantoms were downscaled using two methods; 8 phantoms scaled to nearest lower discrete age and 6 phantoms scaled to median ages based on CCSS participants' ages at RT.

We used two approaches to validate the scaling of phantoms. In the first approach, we compared the overlap and organ displacement parameters between the scaled and ground-truth UF/NCI phantoms at discrete ages. In the second approach, we compared the anthropometric parameters of scaled phantoms with ground-truth phantoms, and with reference data from ICRP 89 (ICRP 2002) and the Center for Disease Control and Prevention (CDC) (Centers for Disease Control and Prevention 2000).

2.4.1 Quantitative assessment of body region/organ overlap and displacements at discrete ages

The main goal of quantifying the overlap and the displacement was to determine the body-regions/organs that are most and least affected by scaling, in terms of their size and position. To quantify the overlap between two ROIs of a body region/organ, we first performed rigid registration between the scaled and ground-truth phantoms at discrete ages using the centroid of the trunk body region. Using built-in functions within RayStation v10B, we calculated the Dice similarity coefficients (DSC) and mean distance to agreement (MDA) for the whole-body, brain, heart, liver, pancreas, and kidneys between the scaled and ground-truth phantoms. The DSC is a measure which calculates the overlap between two ROIs. The values of DSC ranges from 0 to 1 with 0 indicating no overlap and 1 indicating complete overlap (Dice 1945). A DSC value of 0.7-0.8 is considered good agreement (Dice 1945, Mattiucci *et al* 2013, Thomson et al 2014). The MDA estimates the average similarity between the two ROIs by estimating the average of distance between the point per voxel on the surface of two ROIs (Brock *et al* 2017). A value of MDA=0cm represents that the boundaries of two ROI is perfectly overlapped.

To estimate the displacements in the body regions/organs, we calculated the Euclidean distance (ED) between the centroids of the body regions/organs of scaled and ground-truth reference size UF/NCI phantoms using the equation below-

$$ED = \sqrt{\left(x_{c_t} - x_c\right)^2 + \left(y_{c_t} - y_c\right)^2 + \left(z_{c_t} - z_c\right)^2} \quad \textbf{17}$$

where, $(\mathrm{x_c}, \mathrm{y_c}, \mathrm{z_c})$ and $(\mathrm{x_{c_t}}, \mathrm{y_{c_t}}, \mathrm{z_{c_t}})$ are the centroids of body regions/organs ROIs in ground-truth and transformed (scaled) phantom, respectively.

2.4.2 Quantitative assessment of anthropometric parameters at all ages

The goal of assessing the anthropometric parameters was to gauge the standing heights and organ masses of the scaled phantom with respect to reference data. First, we compared the standing heights of the scaled phantoms with those of the ground-truth phantoms at discrete ages and reference data from CDC at all ages. Specifically, we calculated the percent difference (equation (18)) between the standing heights of scaled phantoms, and (1) heights of the ground-truth phantoms, and (2) CDC-reported 50th percentile heights for all 14 scaled phantoms.

$$PD = \frac{S_h - G_h}{G_h} \times 100 \quad \textbf{18}$$

Where, $\mathrm{S_h}$ is the height of a scaled phantom and $\mathrm{G_h}$ is the height from a ground-truth phantom or CDC data.

Second, we compared the scaled organ masses with ICRP 89 reference data. First, we estimated the mass of the scaled organs by taking the product of the organ volumes from RayStation and ICRU 46 reported reference densities (ICRU 1992b). We then calculated the difference between the masses of scaled organs and ICRP 89 reported organ masses. The calculation was performed for brain, heart, lungs, liver, stomach, and kidneys and all of the male and female discrete-aged phantoms, as ICRP 89 data are unavailable for 3.9-, 8.0-, and 9.1-year-old phantoms. For lungs and kidneys, combined masses of left and right organs were compared.

2.5 Difference in organ dose due to scaling- Wilms' Tumor RT plan example

In historic RT cohorts, dose reconstructions are based on treatment parameters abstracted from the RT records, including field size and field location (based on anatomical landmarks). In such studies, patients' heights and weights or CT images are not always available. Thus, if one were to do the dose reconstructions for survivors at continuous-valued ages, the nearest age-matched phantom would be selected, and the coded field would be reconstructed on that phantom. In this scenario, a patient's coded field size would not be adjusted in size for the differences in age between the patient and the closest age-matched phantom. However, in contemporary treatments, RT records include patients' height and weight and CT images at the time of RT. In this scenario, with the anatomical information, the field sizes could be appropriately adjusted to better align with the anatomical landmarks from the RT records. Therefore, in our dosimetric assessment, we considered both scenarios and performed a dosimetric assessment between the exact age-scaled and nearest age-matched discrete-aged phantoms by designing typical RT plans in RayStation TPS for Wilms' tumor as this is one of the common pediatric cancers in the CCSS.

In the first study, we downscaled a reference size 5-year-old phantom to a 3.9-year-old and constructed right flank fields identical in size on both the 3.9-year-old and 5-year-old phantoms. Specifically, 6 MV AP/PA right flank fields were simulated on a 3.9-year-old with the superior field border at 2 cm below the liver/heart boundary, the inferior border at the 5^{th} lumbar vertebrae, the right border at a 1 cm margin enclosing the liver, and the left border enclosing the vertebral bodies. A total of 20Gy was administered to the isocenter placed at midplane in AP/PA direction. We then measured the size of the simulated field and

reconstructed an identical pair of AP/PA flank fields on a 5-year-old phantom. The volume receiving $\geq$ 15Gy (V_{15}), and the mean dose to pancreas, liver, and stomach were calculated. Absolute difference and percent difference were calculated for both phantoms' RT plans.

In the second study, we scaled a cohort of seventeen body size-dependent UF/NCI phantoms (9 male and 8 female) of created from the 5-year-old reference phantom to 3.9-year-old and simulated the same standard Wilms' tumor 3D conformal RT plan on all 34 phantoms. All of the treatment parameters were the same as the 3.9-year-old of the first study except the field size, which varied to maintain identical field borders. Specifically, the superior and inferior field borders were set at 2 cm below the liver/heart boundary and the level of the 5^{th} lumbar vertebrae, respectively. The medial field border was set enclosing the thoracic vertebrae. Dose to organs that were either fully or partially in-beam was calculated. Here, we compared the percent of volume receiving $\geq$ 15 Gy (V_{15}), mean dose, and minimum dose received by 1% (D_1) and 95% (D_{95}) between the 5-year-old phantoms and the corresponding 3.9-year-old phantoms. Organs included the pancreas, liver, stomach, left kidney (contralateral), right kidney, right and left colons, gallbladder, thoracic vertebrae, and lumbar vertebrae. To determine if the dose and dose-volume metrics were significantly different between treatment plans for the different phantoms, we performed a non-parametric Wilcoxon rank sum test using the SciPy package of the Python programming language. Medians, standard deviations, and p-values ($p<0.05$ is significant) are reported for each metric.

3. Results

3.1 Feasibility of scaling UF/NCI phantoms to continuous-valued ages

The feasibility of downscaling the reference size UF/NCI phantoms to any arbitrary age using our ASF and transformation function is demonstrated in Figure 9. The figure shows the downscaled phantoms in standing positions next to their nearest age-matched discrete-aged phantom. An important finding of the scaling is that the structural integrity of the phantoms is maintained after the scaling, i.e., all of the organs and body regions remained intact with no unexpected organ displacement or gaps between body regions

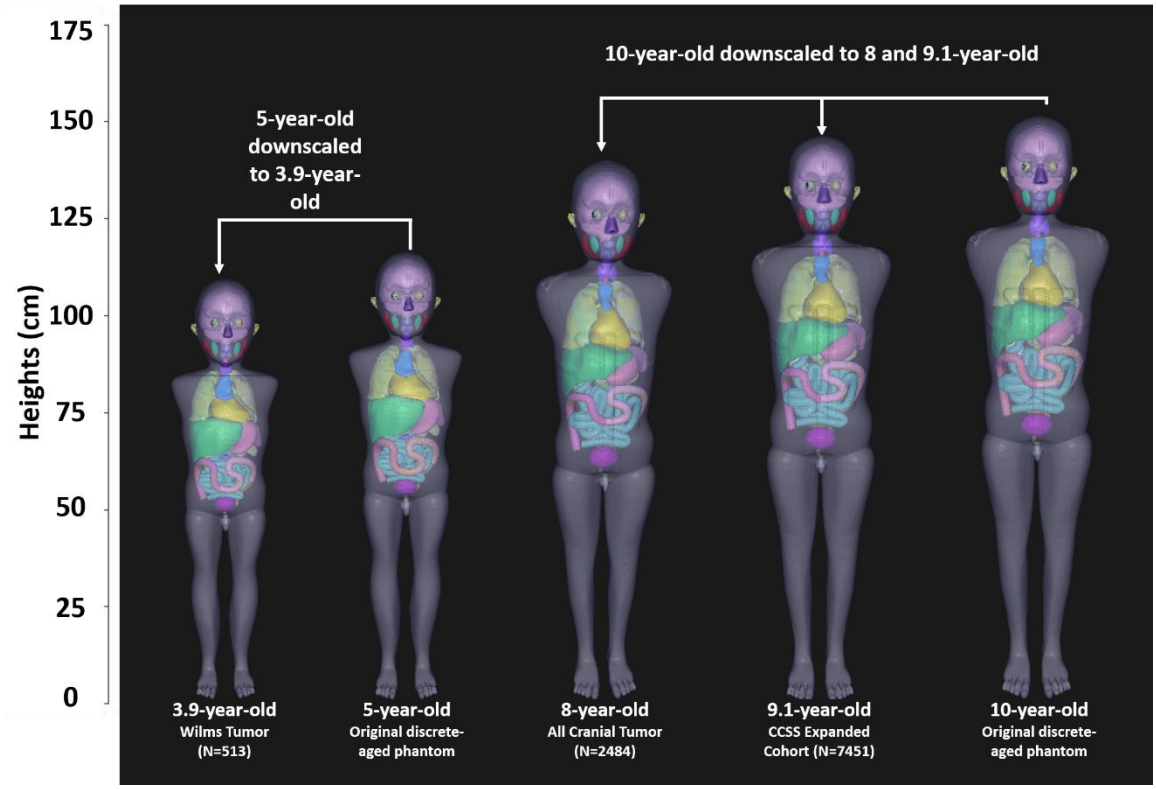

Figure 9: Downscaling of UF/NCI nearest age-matched discrete-aged pediatric male phantoms (5-year-old and 10-year-old phantoms) to median ages (3.9 years for Wilms' tumor, 8 years for all cranial tumors, and 9.1 years for all individuals from the CCSS expanded cohort) of different CCSS cohorts.

3.2 Quantitative assessment of overlaps and displacements due to scaling at discrete ages

The DSC, MDA, and ED between the scaled and ground-truth reference size phantoms at discrete ages for the whole-body ROI and organ ROIs are presented in Figure 10. The whole-body and brain showed good ROI overlap with median (range) DSCs of 0.91 (0.86-0.92) and 0.86 (0.58-0.91), respectively. The heart and liver showed average agreement after scaling with median DSC of 0.70 (0.61-0.78) and 0.74 (0.38-0.80), respectively. The kidneys and pancreas had the poorest overlap agreement with low DSC values of 0.58 (0.45-0.74) and 0.32 (0.01-0.62), respectively.

Additionally, the liver, pancreas, and heart showed larger MDA values (i.e. ROI shape variations) compared to the other organs. Specifically, the median (range) MDA for liver, pancreas, and heart were 0.73cm (0.43-1.79cm), 0.78cm (0.47-2.29cm), and 0.68cm (0.47-1.1cm), respectively, while the median MDAs for the whole body, brain, and kidneys were 0.65cm (0.47-0.93cm), 0.51cm (0.34-1.7cm) and 0.62cm (0.29-0.98cm), respectively. However, those difference are not very meaningful as the box plot overlaps mostly.

The brain showed the smallest range of ED displacements with a median ED of 0.97cm (0.58-3.67), while the pancreas, whole-body, heart, kidneys and liver showed median EDs to 2.03cm (0.72-3.82), 1.35cm (1.04-2.3cm), 1.33cm (0.39-1.9cm), 1.04cm (0.41-2.79cm), and 0.97cm (0.58-4.09cm), in case of whole-body, heart, liver, pancreas and kidneys,

respectively. The liver showed the highest ED displacement (4.09cm) among all organs.

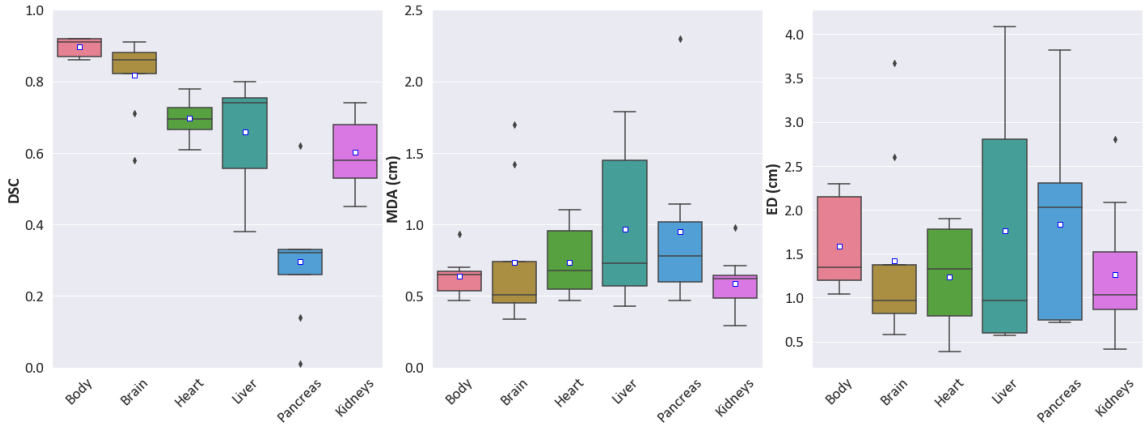

Figure 10: [a] Dice similarity coefficients (DSC), [b] mean distance to agreement (MDA), [c] Euclidean distance (ED) between the scaled and ground-truth phantoms at discrete ages for whole-body and five different organs are shown. Means are represented by white square boxes.

3.3 Comparison of anthropometric parameters

The overall trends in standing heights and the percent difference/absolute difference between the standing heights of the scaled phantom and reference data (UF/NCI and CDC) are shown in Figure 11 and Table 5 at all studied ages. In Table 5, the data are segregated into discrete and continuous-valued ages. Overall, the heights of the scaled phantoms were within 6.3% (6.9cm) of the ground-truth phantom and CDC 50th percentile height data. Better agreement (within 3% or 3.9cm) was observed in the case of the discrete-aged phantom as compared to the phantoms of continuous-valued age.

The scaled masses (in grams) of seven different organs and the absolute difference compared with ICRP 89 reported masses are listed in Table 6 for all the discrete-age scaling.

For all cases, the masses of the brain, pancreas, and kidneys of the scaled phantom were smaller than their ICRP 89 counterparts, as indicated by negative differences. However, the masses of the scaled lungs and stomach were larger than those in the ICRP 89 data. Lastly, except for the 1-year-old phantom, the masses of the scaled heart and liver were smaller than those of the ICRP 89 phantoms. Overall, we obtained an absolute difference ranging from 0.4g to 340g across all of the studied organs and ages.

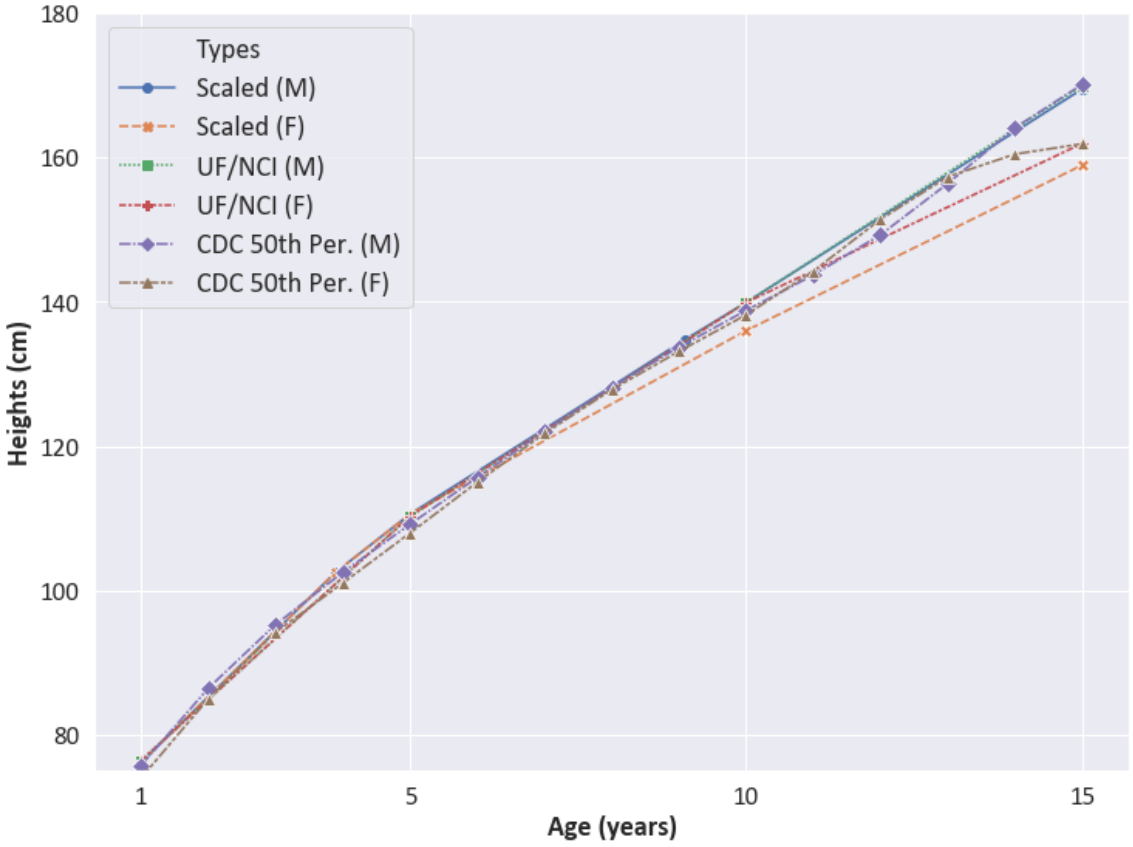

Figure 11: Trend of standing heights of scaled phantoms with respect to original UF/NCI phantoms and CDC reported 50th percentile heights for both male and female.

Table 5. Comparison of standing heights of scaled phantom heights with ground-truth UF/NCI phantom heights and with CDC reported 50th percentile heights

	Scaled Heights (cm)		**Percent Difference (%)**			
Age**	Male	Female	UF/NCI Male*	UF/NCI Female*	CDC Male*	CDC Female*
			Discrete ages			
1 (5)	76.2	76.2	0.4 (0.3)	0.4 (0.3)	0.1 (0.1)	2.4 (1.8)
5 (10)	110.6	110.6	0.3 (0.3)	0.3 (0.3)	1.3 (1.4)	3.0 (3.2)
10 (15)	139.9	136.0	0.0 (0.0)	2.8 (3.9)	0.8 (1.1)	1.3 (1.8)
15 (Adult)	169.5	158.9	0.3 (0.5)	1.9 (3.0)	0.1 (0.2)	1.8 (2.8)
			Continuous-valued ages †			
3.9 (5)	102.6	102.6	6.3 (6.9)	5.5 (5.9)	1.1 (1.2)	2.7 (2.7)
8 (10)	128.3	128.3	4.5 (6.0)	2.8 (3.7)	0.1 (0.2)	0.4 (0.5)
9.1 (10)	134.8	134.8	3.2 (4.5)	1.4 (1.9)	0.5 (0.6)	1.0 (1.3)

**Absolute difference is shown in the parenthesis (in cm). **Original age of the phantom that was used for downscaling is shown in parenthesis i. †Power law fit was used to estimate the ground-truth heights of UF/NCI phantoms for non-discrete ages.*

Table 6: Comparison of scaled organ masses of UF/NCI computational phantoms with ICRP 89 reference masses.Scaled masses and difference between the scaled and ICRP 89 reference masses are reported. All masses are in grams.

1-year-old					5-year-old				10-year-old				15-year-old			
	SM	SF	SM-ICM	SF-ICF	SM	SF	SM-ICM	SF-ICF	SM	SF	SM-ICM	SF-ICF	SM	SF	SM-ICM	SF-ICF
Brain	896.1	896.3	-53.9	-53.7	1158.0	1158.1	-152.0	-21.9	1311.5	1199.5	-88.5	-20.5	1326.7	1196.7	-93.3	-103.3
Heart	125.3	125.3	27.3	27.3	198.4	198.5	-21.6	-21.5	356.0	291.8	-14.0	-78.2	636.4	469.4	-23.6	-70.6
Lungs	106.9	106.9	26.9	26.9	174.3	174.2	49.3	49.2	373.7	357.2	163.7	147.2	669.1	547.9	339.1	257.9
Liver	330.6	330.7	0.6	0.7	451.0	451.2	-119.0	-118.8	714.0	717.1	-116.0	-112.9	1391.5	1082.5	91.5	-217.5
Stomach	77.0	76.9	57.0	56.9	110.0	110.0	60.0	60.0	170.1	175.2	50.1	55.2	306.4	285.7	156.4	145.7
Pancreas	19.6	19.6	-0.4	-0.4	31.4	31.4	-3.6	-3.6	57.5	54.4	-2.5	-5.6	105.2	91.1	-4.8	-8.9
Kidneys	65.7	65.7	-4.3	-4.3	101.3	101.2	-8.7	-8.8	140.9	135.8	-39.1	-44.2	242.1	216.5	-7.9	-23.5

SM=Scaled masses of UF/NCI male phantoms; SF = scaled masses of UF/NCI female phantoms; ICM = ICRP 89 reference masses of male; ICF = ICRP 89 reference masses of female

3.4 Comparison of Wilms' tumor RT plan dose of exact age-scaled and nearest age-matched phantoms

The results of the dosimetric study, in which the same field size and same isocenter were used for the Wilms' tumor treatment plans for a 3.9-year-old downscaled from a reference size 5-year-old and an original unscaled reference size 5-year-old phantom, are reported in Table 7 and Figure 12. The beam's eye view and isodose washes for the 3.9-year-old are shown in 12a and 12c, and those for a 5-year-old are shown in 12b and 12d, respectively. In the isodose washes, dose coverage of the organs differed between the 3.9-year-old and the 5.0-year-old. For example, different fractions of the pancreas and liver are enclosed within the 75% isodose line ($15\ \mathrm{Gy}$). As a result, the absolute differences in V_{15} of pancreas and liver were 3.52% and 5.98%, respectively (Table 7). Results for all organs and dose metrics are listed in table 7.

Results from the dosimetric study where the field borders relative to anatomical landmark were consistent for all phantoms (resulting in different field sizes) are listed in Table 8 and illustrated in Figure 13. V_{15} and mean dose were significantly different between exact age-scaled and nearest age-matched phantom in all other organs except for the right kidney (target), right colon, and gallbladder. The contralateral kidney was significantly different between phantoms in all dose metrics except D_{95}. Similarly, liver and pancreas were significantly different in all except D_1 and D_{95}, respectively. Figure 13 shows the distribution of metrics for selected near beam organs; pancreas, liver, contralateral kidney, and stomach. In all organs and metrics, the median and mean were higher in the case of the original 5-year-old phantom.

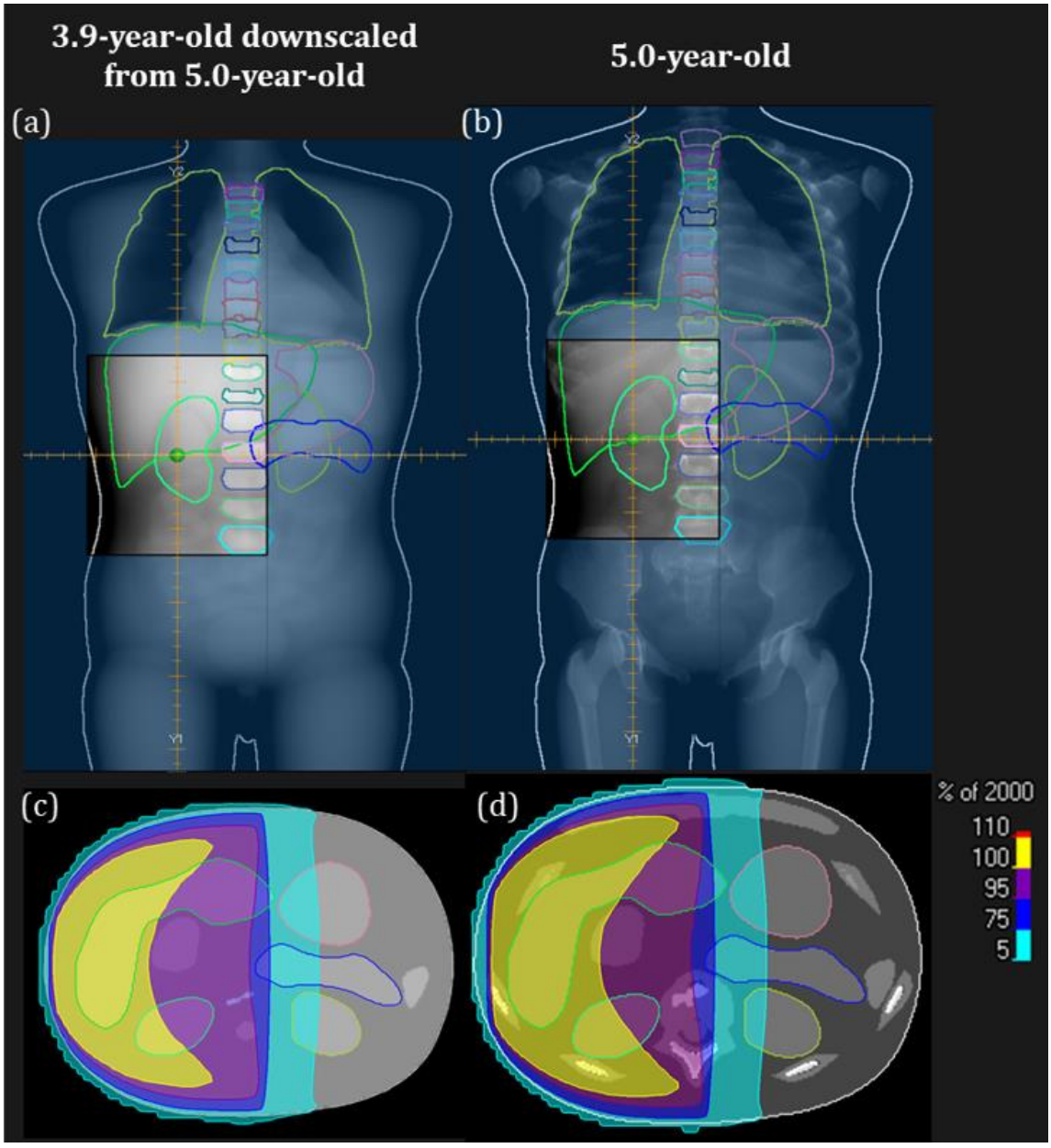

Figure 12: Digitally reconstructed radiograph of a Wilms' tumor plan for (a) a 3.9-year-old downscaled from a reference size 5-year-old and (b) an unscaled reference size 5-year-old. Isodose wash for liver, stomach, kidneys, and pancreas of (c) the downscaled and (d) the unscaled phantoms for 5% (cyan), 75% (blue), 95% (purple), 100% (yellow), and 110% (red) of the prescription dose. Except vertebral bodies, no bones were downscaled.

Table 7: Absolute and percent difference between the V_{15} and mean dose from 6MV Wilms' tumor RT plan (20 Gy to right kidney) between unscaled reference size 5-year-old and 5-year-old downscaled to 3.9-year-old

	V15, in %		Mean Dose, Gy	
Organs	Abs. diff	% diff	Abs. diff	% diff
Pancreas	3.52	42.04	0.85	4.25
Liver	5.98	8.61	1.29	6.45
Stomach	0.00	0.00	0.11	0.55

% difference in mean dose is normalized to 20 Gy

Table 8: Metrics investigated to establish the difference in dose from 6 MV Wilms' tumor RT plan (20 Gy to right kidney) in between 3.9-year-old and 5.0-year-old phantoms. Wilcoxon rank sum test was performed to determine if differences were statistically significant ($p<0.05$ is significantly different)

	V_{15} (in %)			Mean Dose (Gy)			D_1 (Gy)			D_{95} (Gy)		
	3.9y Med.	5.0y Med.	P-Val	3.9y Med.	5.0y Med.	P-Val	3.9y Med.	5.0y Med.	P-Val	3.9y Med.	5.0y Med.	P-Val
Pancreas	16.86	19.55	<0.05	4.40	4.75	<0.05	19.13	19.15	>0.05	0.32	0.33	>0.05
Liver	66.68	70.71	<0.05	14.38	14.86	<0.05	20.97	21.02	>0.05	1.20	1.32	<0.05
Lt. Kidney	0.01	0.40	<0.05	1.55	1.78	<0.05	9.31	10.78	<0.05	0.72	0.73	>0.05
Rt. Kidney	100.00	100.00	>0.05	20.07	20.11	>0.05	20.62	20.68	>0.05	19.60	19.62	>0.05
Rt. Colon	68.08	67.63	>0.05	14.66	14.60	>0.05	21.29	21.35	>0.05	0.59	0.58	>0.05
Lt. Colon	15.30	15.90	<0.05	4.14	4.36	<0.05	19.76	19.84	>0.05	0.30	0.30	>0.05
Stomach	0.44	0.59	<0.05	0.87	0.99	<0.05	7.59	9.56	<0.05	0.29	0.30	>0.05
Gallbladder	100.00	100.00	>0.05	19.78	19.80	>0.05	20.00	20.03	<0.05	19.57	19.58	>0.05
T. Vertebra	14.29	15.50	<0.05	3.08	3.37	<0.05	19.32	19.35	>0.05	0.00	0.00	<0.05
L. Vertebra	97.81	98.47	<0.05	18.96	19.04	<0.05	19.95	20.00	>0.05	17.29	17.50	>0.05

V_{15} = percent of volume receiving $\geq$ 15Gy; D_1 is dose received by 1% of the volume; D_{95} is dose received by 95% of the volume. Blue label highlights the significantly different cases; Rt. and Lt. colon stands for right and left colon respectively. T. and L. vertebra stands for thoracic and lumbar vertebra. Med. indicates median.

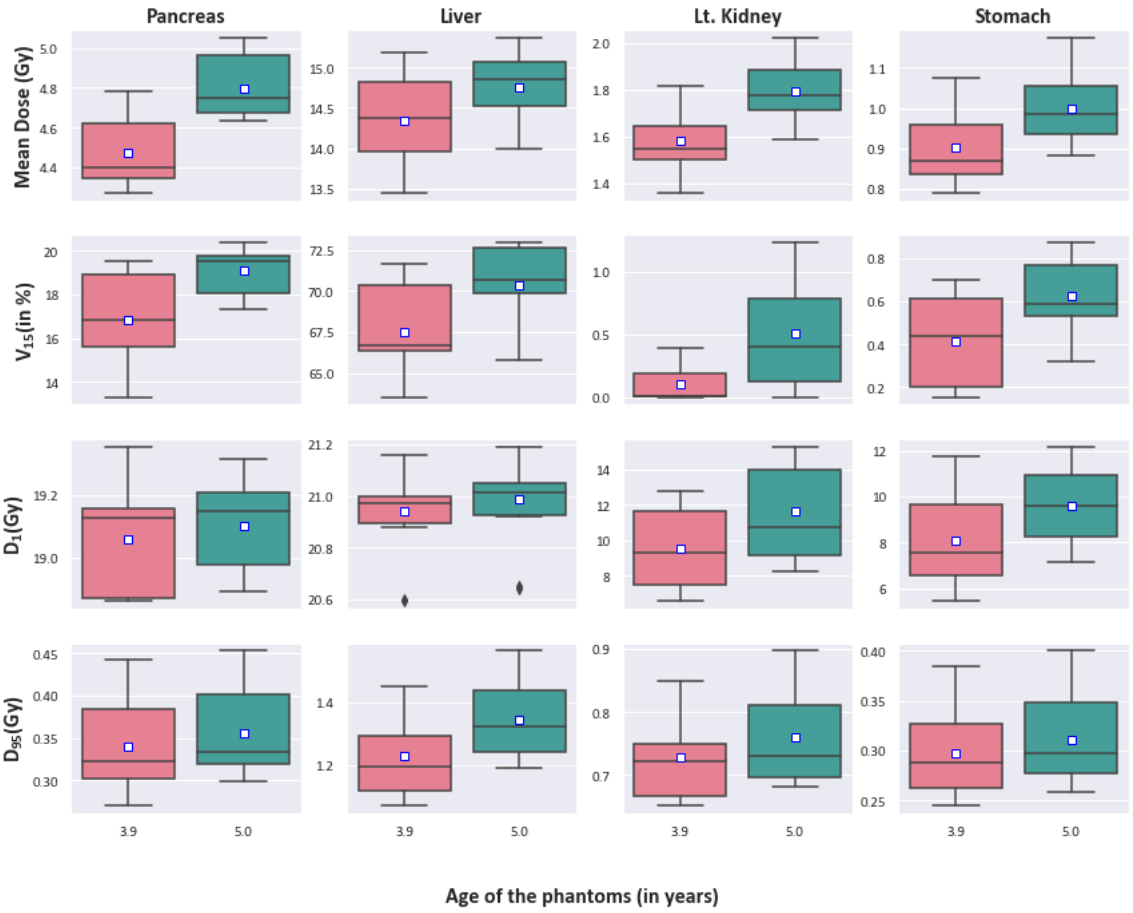

Figure 13: Boxplot showing the V_{15}, mean dose, D_1, and D_{50} for pancreas, liver, left kidney, and stomach. All of the results presented here are significantly different ($p<0.05$, N=17) except D_{95} for left kidney, D_1 for the liver, and D_{95} for the stomach. Mean is represented by the white box.

4. Discussion

In this study, we have successfully scaled the realistic CT-based UF/NCI pediatric reference phantom to arbitrary ages using our ASFs, which is also a proof-of-concept that our ASFs can be used to accurately scale any CT-based anatomy. We have also established that dose to organs in between the cohorts of age-specific (continuous-valued age) and nearest discrete age-matched phantoms varies significantly ($p<0.05$). This is an indication that using an exact age-scaled phantom is an important consideration for dose reconstruction studies. Our ASFs are functions of age, direction and body region, and are primarily used in retrospective organ dose reconstruction studies where phantom or patient's anatomy must be generated at the time of RT. Currently, there exists a different types of protocols for selecting phantom as surrogate anatomy: one would select phantom by matching the heights and weights of the patient or select the nearest age phantom or select the phantom based on the anthropometric parameter of the trunk from the CT scan at the time of treatment (Whalen *et al* 2008, Kuzmin *et al* 2018). However, for retrospective studies such as in the CCSS (N>13000 with RT) where patients were treated in the pre-CT era, age is the only most common, and often the only anthropometric parameter that is available retrospectively. In such a many case, matching the height and weight of the phantom or matching the anthropometric parameter of the trunk is not feasible. One would attempt to select a nearest-age phantom instead of a continuous-valued age phantom; however, such protocols are associated with higher uncertainties in organ shape and size/volume, that can translate to uncertainty in organ dose reconstruction and hence in risk assessment (Kry *et al* 2007, Whalen *et al* 2008, Morton *et al* 2013). Our age scaling methodologies overcome these limitations as they can accurately scale any phantom of choice or CT-based anatomy to the

patient's age at the time of treatment. Furthermore, our ASFs roughly require 3 minutes to scale a phantom in TPS which also ensures it suitability in the large cohorts. Lastly, our ASFs have been used to scale our in-house phantoms for other cohorts such as the St. Jude Lifetime, Adult Life after Childhood Cancer in Scandinavia, and the Dutch Childhood Oncology Group over three-decade (listed in Howell *et al* (2019)).

Our feasibility study showed reasonable accuracy in the context of overlap and displacement metrics for the whole body and various organs. While the whole-body and brain showed the best DSC scores, the heart and liver scores were still acceptable as they showed median DSCs of 0.69 and 0.73, respectively which means 50% of the distribution are >0.7 which is considered a good DSC values (Dice 1945, Zou *et al* 2004). As reported in section 3.2, the pancreas and kidneys showed poor DSC agreement as the median DSCs were at 0.32 and 0.58, respectively, but this cannot be solely attributed to an error in transformation and scaling as the heart and liver should have also shown poor agreement because all organs in trunk use same scaling factors. It is important to note that the UF/NCI phantoms at different ages are not from the same/single patient, which introduces inter-patient variation in in organ shape, size, and position (Lee *et al* 2010). Furthermore, another reason could be attributed to the sensitivity of DSC to the volume of the organ. For example, a 1 cm displacement could affect the pancreas/kidneys more than the brain which has a larger volume. The large ED for the liver and pancreas in our study was not unexpected as studies of adult patients have reported high range of motion for these organs. One study reported motion of up to 5.7 cm in the liver (Davies *et al* 1994, Langen and Jones 2001), while another study reported motion of up to 8 cm in liver and pancreas (Suramo *et al* 1984,

Langen and Jones 2001). This organ displacement also contributed to the poor agreement we observed in DSC and MDA.

In the anthropometric assessment of scaled phantoms, the scaled standing heights agreed within 6.3% (6.9 cm) of the reference data. Higher disagreements data were confined to continuous-valued ages, likely because we used a power law to interpolate the heights of the UF/NCI phantoms at discrete ages to obtain heights at continuous-valued ages. With regard to organ masses, we observed ICRP 89 masses were greater than scaled organ masses except for the stomach and lungs, where ICRP 89 is smaller. Although the scaled masses highly deviated from the ICRP 89 masses, the scaled masses for organs such as the brain, lungs, liver, and kidneys for 1-, 5-, and 10-year-old are well within the range of masses reported in the US population autopsy study by Molina *et al* (2019).

For the dose study, our investigation using the same field size on exact age-scaled versus nearest age-matched phantoms showed differences in V_{15} and mean dose up to 6% and 1.3 Gy (6.45%), respectively. We used the same field size because, in retrospective dose reconstruction, one would not modify the original field size when using an age-matched phantom instead of an exact-age phantom. The reason behind the differences is mostly the shape and position of the organs which varied across exact age-scaled and nearest age-matched phantom. In dose reconstruction studies, it has been found that organ shape, volume, position, dose reconstruction method, irradiation sources, etc. are the major sources of uncertainty in dose estimation. Furthermore, Kry *et al* (2007) estimated that a 50% uncertainty in dose estimation could result in a significant difference in risk of a second cancer. Therefore, an uncertainty of 6% in V_{15} or 6.45% in mean dose can potentially affect the risk estimation studies when they are combined with other sources of uncertainties.

Additionally, a difference of 1.3 Gy can also affect the risk estimation study if the doses are finely binned and organ dose values (not the difference) falls at the edge of the bin. Those impacts will be pronounced when the cohort size is large. Furthermore, it is also important to determine the effect of scaling on the field size and hence on the organ dose. Our second study showed that V_{15} and mean dose were significantly different ($p<0.05$) except for the organs that are fully inside the beam. This result was expected because those organs received roughly 100% of the prescribed dose in each case.

While we have successfully demonstrated the feasibility of scaling the phantoms to any arbitrary age using our in-house ASFs and have established the difference in dose between exact-age and nearest age-matched phantoms, our study also revealed that our ASFs need enhancements. Specifically, in the current study, the underestimation and overestimation of the organ masses (as shown in Table 6) suggest our ASFs could be enhanced with organ-specific ASFs in addition to our current body region-specific ASFs. However, it is worthwhile to highlight that the scaled masses fell within the range of autopsy masses as discussed earlier.

Our current ASF-related enhancement includes the development of scaling factors based on the percentile height of the U.S. population. We are combining our ASFs and CDC-reported percentile specific-heights to generate percentile specific ASFs. This will allow us to scale the phantom based on these heights, which will be available in modern CCSS cohorts. For modern cohorts in the CCSS, the survivor data will be present in the CT scans, where we can measure body region-specific parameters such as size, volume, and circumference. We can use those parameters to estimate the BMI of the patients and develop modulation factors to generate cohort-specific ASFs. Finally, our group is enhancing/developing individual

organs (e.g. heart, colon, etc.) within our in-house phantom, which involves the incorporation of modulation factors into scaling methodologies. For example, Shrestha *et al* (2020) introduced a modulation factor based on inherent differences in the trunk size of a UF/NCI phantom and an MDA phantom to develop a new CT-based hybrid heart before integrating it into the generic phantom.

5. Conclusion

We have successfully implemented our ASFs to scale UF/NCI phantoms from one age to another age and have validated the scaling process with reasonable accuracy in terms of geometric and anthropometric parameters. We have also established that there exists a significant difference in dose to organ between populations of exact age-scaled continuous-valued phantoms and nearest age-matched discrete aged phantoms. The implementation and validation allow us to scale - UF/NCI phantoms or any CT-based patient anatomy for RT epidemiological study using cohorts where age is the main parameter.

Chapter 5: Discussions and Conclusion

1. General Overview

The primary purpose of this thesis was to implement our FORTRAN phantom and its ASFs in DICOM format within a commercial TPS so that our dose reconstruction methods can be used to estimate organ doses of survivors treated with contemporary RT plans. Our central hypothesis was to implement the phantom within 3% of the FORTRAN phantom with scaled heights within 7% of the CDC reported 50th percentile heights. To achieve our purpose, we established two specific aims, all of which were successfully completed by developing several Python scripts in RayStation TPS.

Our first aim was to accurately model and validate our computational phantom and its ASFs in DICOM format. We validated our implementation by calculating percent differences in corner points, volume, and scaled heights of the DICOM phantom and reference data. All of the metrics were well within limits set in our central hypothesis. Most of the discrepancies in modeling were attributed to the removal of the negligible gap present in between the body regions of our generic phantom. The conversion of our organs from point form to surface contours enabled us to estimate dose to organ ROIs for the first time. Our dose metrics for partially in-beam organs from TPS agreed within 0.07Gy (mean dose) of the results from the fully validated in-house dose calculation method. That supported our hypothesis that our phantom is ready to be used for dose calculation studies within a TPS.

The validation of our ASFs in aim 1 inspired us to scale other whole-body CT-based phantoms using our age-scaling methodologies. We adopted UF/NCI phantoms to test the feasibility and successfully scaled the phantoms to arbitrary ages using our ASFs. To assess

the dosimetric impact of scaling, we designed a study in which we constructed standard Wilms' tumor plan of a CCS on an exact age-scaled phantom and the nearest age-matched phantom. The phantom selection based on a nearest anthropometric parameter such as age is pretty standard when the exact age phantom is unavailable. Our study showed this could lead to uncertainty in dose metrics such as up to 6% and 1.3Gy in V_{15} and mean dose, respectively, when field size was kept the same between the two phantom types. Since the risk-assessment studies report doses in bins, a difference of 6% or 1.3Gy alone could not affect the risk-assessment results. However, the dose-reconstruction methodologies include uncertainties due to various sources, as reported in Vũ Bezin *et al* (2017) and Xu *et al* (2008). Therefore, a 6% uncertainty in combination with other sources could exceed a total uncertainty of 50%, which has been estimated to affect risk-assessment studies significantly (Kry *et al* 2007, Vũ Bezin *et al* 2017).

2. Project Limitation and Future Directions

A retrospective analysis of our two aims revealed several aspects of projects that can be improved. First, in aim one and aim 2, we found that the scaled organ masses were smaller than the masses from reference phantoms and autopsy. In aim 2, most of the discrepancies in height were confined to female data. Such discrepancies could be improved if we have ASFs specific to the population's organ, sex, and percentile height. A preliminary study has already been conducted to develop percentile-specific ASFs. We modified our ASFs in AP, IS, and RL by using modulation factors that would match the scaled heights of the phantom to CDC-reported percentile-specific heights at discrete ages. Figure 14 and 15 shows the preliminary results of using percentile specific ASFs.

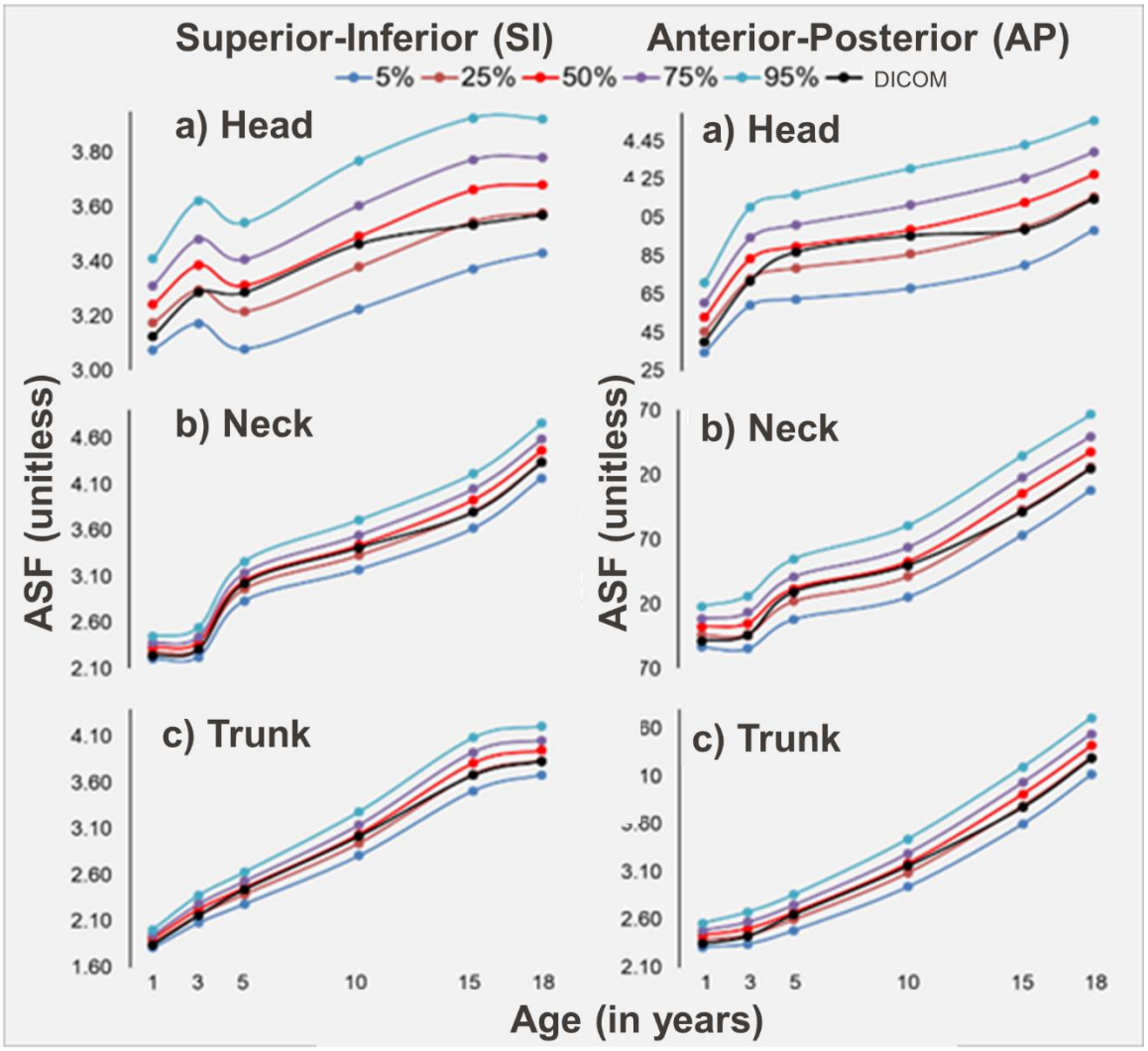

Figure 14: Evolution of ASFs as a function of age and percentile heights for different ages.

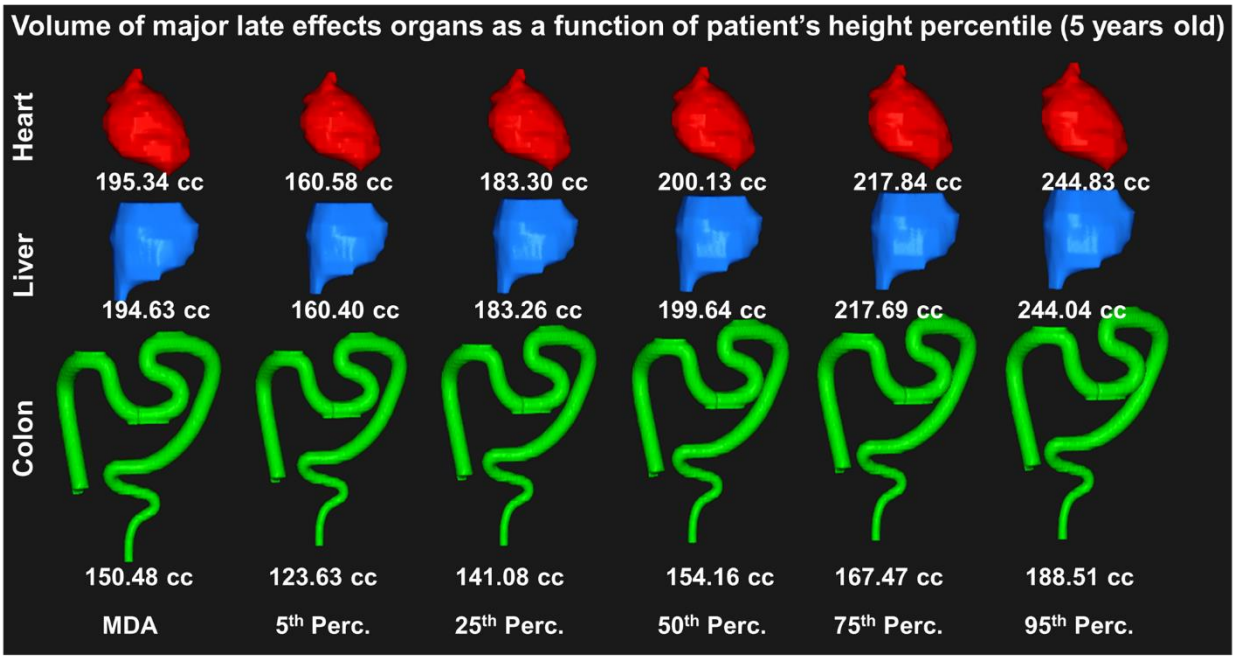

Figure 15: Change in the volume (volume is shown in white) of heart, liver, and colon (test model) as a percentile-based ASF function is shown for 5-year-old.

Another project that we would like to work on is the use of ASFs to scale ICRP 143 pediatric reference phantom. ICRP 143 adopted the reference size UF/NCI phantom, which makes the phantom standard for use in dosimetry studies. Several modifications, such as the development of organ substructures, the addition of lymph nodes, and overall enhancement, were performed before ICRP adopted this phantom. A visual comparison between two phantoms at five years of age is shown in Figure 16, which shows the advancement of anatomy. Therefore, using ASFs to scale the organs with substructure will be a new addition to our current feasibility studies.

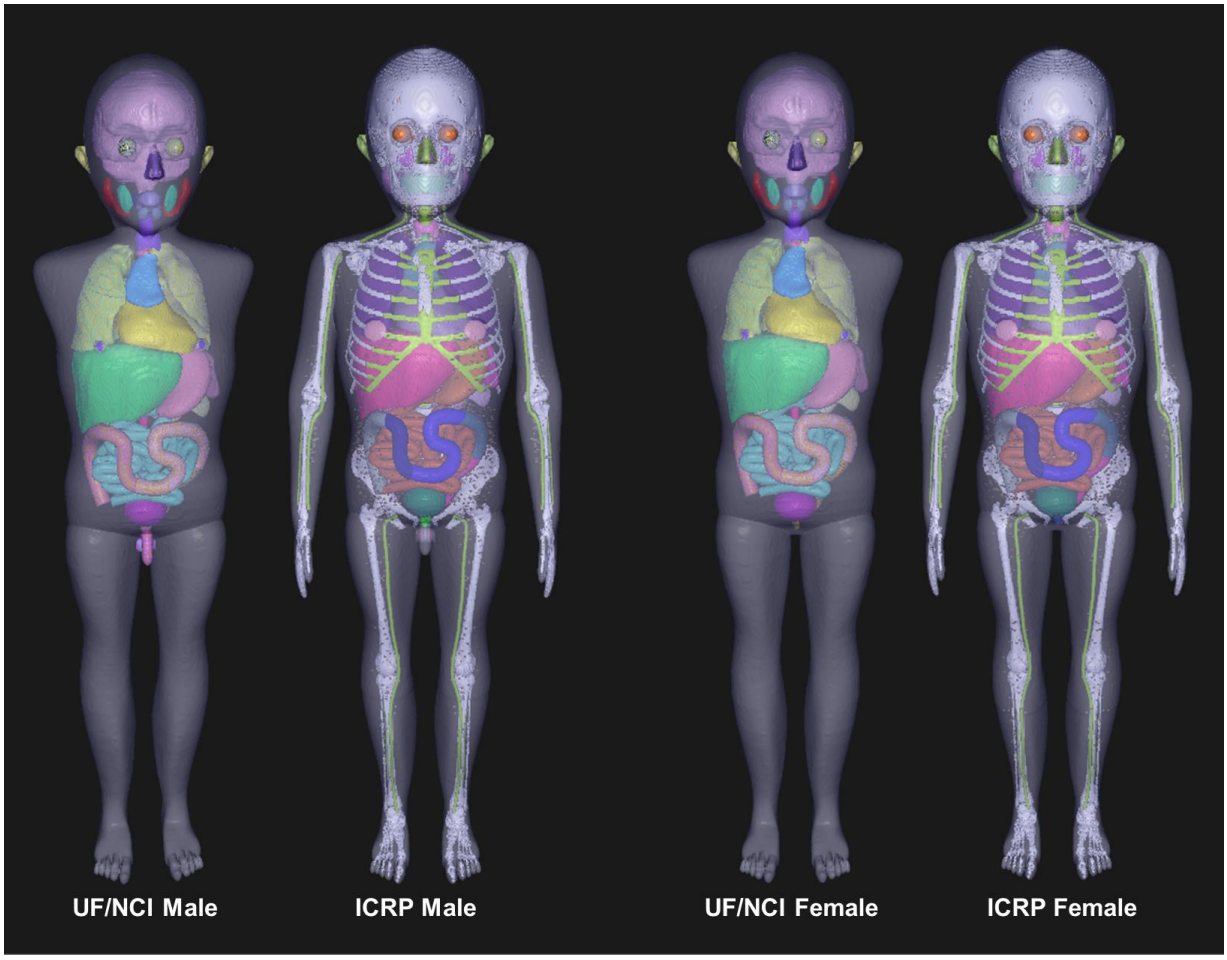

Figure 16: Comparison of a 5-year-old ICRP 143 and UF/NCI male and female phantoms (armless version)

Another major study that our group would like to calculate the accuracy of out-of-field dose in the RayStation treatment planning system. Such studies are essential because, for late effects studies, near beam and far beam organs are of significant interest and TPS are not accurate for those organs. The quantification of accuracy will allow us to incorporate modulation factors in our dose-reconstruction method for cohorts treated with contemporary RT. A previous study from our group was conducted for Pinnacle TPS when primarily used in our clinic (Howell *et al* 2010a).

3. Conclusion

Our results show that we have accurately implemented our computational phantom and its ASFs in the DICOM format. The phantom and ASFs can be used for dose calculation of studies. We have also validated that our ASFs can be used to scale whole-body CT-based anatomy. One major recommendation that this thesis project suggests is using exact age-scaled phantom over nearest matched phantom in dose reconstruction studies is an important consideration.

Appendices

Appendix A: Mathematical calculations showing transformation of our generic phantom to 7.0-year-old phantom

This appendix is obtained from the following peer-reviewed publication:

A.C. Gupta, S. Shrestha, C.A. Owens, S.A. Smith, Y. Qiao, R.E. Weathers., P.A. Balter, S.F. Kry, and R.M. Howell, "Development of an age-scalable 3D computational phantom in DICOM standard for late effects studies of childhood cancer survivors," Biomedical Physics and Engineering Express. Volume 6, Issue 6, pages 1-15. © IOP Publishing Ltd.

We present a sample calculation following the steps in Figure 3 to illustrate how our generic "adult" phantom is transformed to a 7.0-year-old phantom. Due to the symmetric nature of a cube, if two corner points describing a diagonal of the cube are known, then we can calculate the remaining six corner points of the cube. Hence, we only present the transformation of two opposite corner points for each of the phantom's cuboidal body regions. Additionally, we illustrate the transformation of one point in an organ within the trunk body region.

Step 1: Import Data

In this step, we import the organ points and corner points of the body region from the FORTRAN generic phantom into a DICOM file present in RayStation. To begin, $\mathrm{p_r}$ and $\mathrm{q_r}$ represent the two opposite corners of the cube. Here r ϵ {upper head (uh), lower head (lh), neck (n), trunk (tr), arms (ar), legs (lg)}. The body regions with their opposite corner points are presented in the table below.

Table 9: Opposite corner points describing the main diagonal of each body region in the generic phantom. The corner points are scaled and translated using equations (1) through (6) to obtain the phantom of age $\mathbf{a}$.

Head (upper and lower)	$\mathrm{p_{uh}}(-2.30, 1.00, 0.00)$ and $\mathrm{q_{lh}}(2.30, 6.70, 4.80)$
Neck	$\mathrm{p_n}(-1.20, 6.70, 1.10)$ and $\mathrm{q_n}(1.20, 7.60, 3.50)$
Trunk	$\mathrm{p_{tr}}(-4.00, 7.60, 0.10)$ and $\mathrm{q_{tr}}(4.00, 24.00, 4.90)$
Leg	$\mathrm{p_{lg}}(-2.80, 24.00, 1.10)$ and $\mathrm{q_{lg}}(2.80, 43.20, 3.60)$
Arm*	$\mathrm{p_{ar}}(4.00, 8.00, 1.60)$ and $\mathrm{q_{ar}}(5.60, 21.60, 3.20)$

* In table 9, we present the calculation for the right arm only due to symmetry in approach.

To illustrate how organ points are transformed, we chose the point (-3.40, 14.30, 2.60) in the liver.

Step 2: Select Phantom Age

Here, we select the age of the phantom as 7.0 years.

Step 3: Transform Coordinates

Based on the user-specified age, we use equations (1) through (6) to transform the points of the generic phantom to a phantom of age 7.0 years. The process can be divided into two phases, (i) calculation of the scaling factor and (ii) scaling/translation of generic phantom points.

In phase (i), we identify the age group and access the preloaded scaling factor data for the lower and upper age bounds. Here, the age of 7.0 years falls within the category [5, 10). To calculate the scaling factor for 7.0 years, we use equation (2), which requires the scaling factors for upper and lower age bounds (a_{-}). The scaling factors corresponding to $\mathrm{a}_{-} = 5.0$ and $\mathrm{a}_{+} = 10.0$ for each body region are presented in Table 10.

Table 10: Scaling factors corresponding to the ages of 5.0 and 10.0 years are shown as age=7.0 ϵ [5.0,10.0)

	Age = 5.0 (LR (x), SI (y), AP (z))*	**Age = 10.0 (LR (x), SI (y), AP (z))***
Head	(3.022, 3.286, 3.872)	(3.130, 3.464, 3.957)
Neck	(3.292, 3.026, 3.292)	(3.500, 3.410, 3.500)
Trunk	(2.250, 2.442, 2.653)	(2.750, 3.018, 3.163)
Leg	(3.750, 2.474, 3.840)	(4.583, 3.411, 5.120)
Arm	(3.125, 2.647, 3.125)	(4.000, 3.493, 4.000)

*LR=Left to Right, SI=Superior to Inferior, AP=Anterior to Posterior directions

$$\mathbf{F_{cont}(x, uh, 7) = F_{dis}(x, uh, 5) + \frac{7.0 - 5.0}{10.0 - 5.0}\left(F_{dis}(x, uh, 10) - F_{dis}(x, uh, 5)\right)}$$

$$\mathrm{F_{cont}(x, uh, 7) = 3.022 + \frac{7.0 - 5.0}{10.0 - 5.0}(3.130 - 3.022) = 3.065}$$

The above calculation is repeated in all three directions for each body region, and we finally obtain all scaling factors for age 7.0 years (Table 11). For the organ points, the same calculations are repeated based on the body region in which the organ point lies.

Table 11: Scaling factors for each body region to scale the phantom from generic to age 7.0 years

	$(\mathbf{LR}\ (\mathbf{x}), \mathbf{SI}\ (\mathbf{y}), \mathbf{AP}\ (\mathbf{z}))\ *$
Head	(3.065, 3.357, 3.906)
Neck	(3.375, 3.180, 3.375)
Trunk	(2.450, 2.672, 2.857)
Leg	(4.083, 2.849, 4.352)
Arm	(3.475, 2.985, 3.475)

*LR=Left to Right, SI=Superior to Inferior, AP=Anterior to Posterior directions

In phase (ii), the body region corner points and the organ points are transformed using equations (3) and (6). The transformation of each body region is shown in the subsections below.

Transformation of the head corner points:

For $p_{uh}(-2.30, 1.00, 0.00)$:

$$x_t = x \cdot F_{cont}(x, r, a) = -2.30 \cdot 3.065 = -7.05 \text{ cm}$$

$$y_t = \sum_{r=uh}^{uh} l_{uh} \cdot F_{cont}(y, uh, 7) \quad = (y - y_{sbr}) \cdot F_{cont}(y, uh, 7) = (1.00 - 1.00) \cdot 3.357$$

$$= 0.00 \text{ cm}$$

$$z_{shift} = \frac{Z_{head} \cdot F(z, uh, 7) - Z_{head} \cdot F(z, uh, 7)}{2} = 0.00$$

$$z_t = \left(z - z_{abr_r}\right) \cdot F(z, uh, 7) + z_{shift} = 0.00 \cdot 3.906 = 0.00 \text{ cm}$$

For $q_{uh}(2.30, 6.70, 4.80)$:

$$x_t = 2.30 \cdot 3.065 = 7.05 \text{ cm}$$

$$y_t = \left(y_{ibr_{uh}} - y_{sbr_{uh}}\right) \cdot F_{cont}(y, uh, 7) + \left(y - y_{ibr_{uh}}\right) \cdot F_{cont}(y, n, 7)$$

$$= (3.80 - 1.00) \cdot 3.357 + (6.70 - 3.80) \cdot 3.180 = 18.62 \text{ cm}$$

$$z_{shift} = \frac{Z_{head} \cdot F(z, uh, 7) - Z_{head} \cdot F(z, uh, 7)}{2} = 0.00$$

$$z_t = 4.80 \cdot 3.906 = 18.75 \text{ cm}$$

Transformation of the neck corner points:

For $p_n(-1.20, 6.70, 1.10)$:

$$x_t = -1.20 \cdot 3.375 = -4.05 \text{ cm}$$

Since the superior boundary of the neck on the y-axis is the same as the inferior boundary of the lower head, the transformed point is the same as that obtained for the lower boundary of the head on the y-axis.

$$z_{shift} = \frac{Z_{head} \cdot F(z, uh, a) - Z_n \cdot F(z, n, a)}{2}$$

$$= \frac{(4.70 - 0.00) \cdot 3.906 - (3.50 - 1.10) \cdot 3.375}{2}$$

$$= 5.13 \text{ cm}$$

$$z_t = (1.10 - 1.10) \cdot 3.375 + 5.13 = 5.13 \text{ cm}$$

For $q_n(1.20, 7.60, 3.50)$:

$$x_t = 1.20 \cdot 3.375 = 4.05 \text{ cm}$$

$$y_t = \left(y_{ibr_{uh}} - y_{sbr_{uh}}\right) \cdot F_{cont}(y, uh, 7) + \left(y_{ibr_{lh}} - y_{sbr_{lh}}\right) \cdot F_{cont}(y, n, 7) + \left(y - y_{sbr_n}\right) \cdot F_{cont}(y, n, 7)$$

$$= (3.80 - 1.00) \cdot 3.357 + (6.70 - 3.80) \cdot 3.180 + (7.60 - 6.70) \cdot 3.180$$

$$= 21.48 \text{ cm}$$

$$z_t = (3.50 - 1.10) \cdot 3.375 + 5.13 = 13.23 \text{ cm}$$

Transformation of the trunk corner points:

For $p_{tr}(-4.00, 7.60, 0.10)$:

$$x_t = -4.00 \cdot 2.450 = -9.80 \text{ cm}$$

$$y_t = 21.48 \text{ cm}$$

$$Z_{shift} = \frac{4.70 \cdot 3.906 - 4.90 \cdot 2.857}{2} = 2.18 \text{ cm}$$

$$z_t = (0.10 - 0.10) \cdot 2.857 + 2.18 = 2.18 \text{ cm}$$

For $q_{tr}(4.00, 24.00, 4.90)$:

$$x_t = 4.00 \cdot 2.450 = 9.80 \text{ cm}$$

$$y_t = \left(y_{ibr_{uh}} - y_{sbr_{uh}}\right) \cdot F_{cont}(y, uh, 7) + \left(y_{ibr_{lh}} - y_{sbr_{lh}}\right) \cdot F_{cont}(y, n, 7) + \left(y_{ibr_n} - y_{sbr_n}\right) \cdot F_{cont}(y, n, 7) + \left(y - y_{sbr_{tr}}\right) \cdot F_{cont}(y, tr, 7)$$

$$= (3.80 - 1.00) \cdot 3.357 + (6.70 - 3.80) \cdot 3.180 + (7.60 - 6.70) \cdot 3.180 + (24.00 - 7.60) \cdot 2.672 = 65.30 \text{ cm}$$

$$z_t = (4.90 - 0.10) \cdot 2.857 + 2.18 = 15.89 \text{ cm}$$

Transformation of the leg corner points:

For $p_{lg}(-2.80, 24.00, 1.10)$ and $q_{lg}(2.80, 43.20, 3.60)$:

The transformed x- and z-coordinates of the leg volume are the same as the transformed x- and z-coordinates of the trunk. This was done because we have one leg volume in the phantom. To prevent the leg volume lying outside the xz plane of the trunk when the phantom is scaled to higher ages, we used the same scaling in the xz direction as for the trunk. The length of the leg in the y direction is calculated using equation (4).

For $p_{lg}(-2.8, 24.0, 1.1)$:

$$y_t = 65.30 \text{ cm}$$

For $q_{lg}(2.80, 43.2, 3.60)$:

$$\begin{aligned} y_t = {} & \left(y_{ibr_{uh}} - y_{sbr_{uh}}\right) \cdot F_{cont}(y, uh, 7) + \left(y_{ibr_{lh}} - y_{sbr_{lh}}\right) \cdot F_{cont}(y, n, 7) + \left(y_{ibr_n} - y_{sbr_n}\right) \\ & \cdot F_{cont}(y, n, 7) + \left(y_{ibr_{tr}} - y_{sbr_{tr}}\right) \cdot F_{cont}(y, tr, 7) + \left(y - y_{sbr_{lg}}\right) \\ & \cdot F_{cont}(y, lg, 7) \\ & = (3.80 - 1.00) \cdot 3.357 + (6.70 - 3.80) \cdot 3.180 + (7.60 - 6.70) \cdot 3.180 \\ & + (24.00 - 7.60) \cdot 2.672 + (43.20 - 24.00) \cdot 2.894 = 120.01 \text{ cm} \end{aligned}$$

Transformation of the arm corner points:

For $p_{ar}(4.00, 8.00, 1.60)$:

On the x-axis, the arm starts at the same x-coordinate at which the trunk volume ends. Thus, $x_t = 9.80$ cm. On the y-axis, the volume starts at the same y-coordinate as the trunk.

$$z_t = (1.60 - 1.60) + \frac{(4.70 - 0.00) \cdot 3.906 - (3.20 - 1.60) \cdot 3.475}{2} = 6.40 \text{ cm}$$

For $q_{ar}(5.60, 21.60, 3.20)$:

$$x_t = 5.60 \cdot 3.475 = 19.46 \text{ cm}$$

$$y_t = \left(y_{ibr_{uh}} - y_{sbr_{uh}}\right) \cdot F_{cont}(y, uh, 7) + \left(y_{ibr_{lh}} - y_{sbr_{lh}}\right) \cdot F_{cont}(y, n, 7) + \left(y_{ibr_n} - y_{sbr_n}\right)$$
$$\cdot F_{cont}(y, n, 7) + (y - y_{sbr_{ar)}} \cdot F_{cont}(y, ar, 7)$$
$$= (3.80 - 1.00) \cdot 3.357 + (6.70 - 3.80) \cdot 3.180 + (7.60 - 6.70) \cdot 3.180$$
$$+ (21.60 - 8.00) \cdot 2.985 = 62.08 \text{ cm}$$
$$z_t = (3.20 - 1.60) \cdot 3.475 + 6.40 = 11.96 \text{ cm}$$

Transformation of organ points:

The scaling and translation of organs is performed in the same way as the body regions in which they are located. For example, we present here the scaling of one of the points of the liver, which is present in the trunk region. The sample calculation for the point (-3.40, 14.30, 2.60) in the liver is shown below:

$$x_t = -3.40 \cdot 2.450 = -8.33 \text{ cm}$$

$$y_t = (3.80 - 1.00) \cdot 3.357 + (6.70 - 3.80) \cdot 3.180 + (7.60 - 6.70) \cdot 3.180$$
$$+ (14.30 - 7.60) \cdot 2.672 = 39.39 \text{ cm}$$

$$z_t = (2.60 - 0.10) \cdot 2.857 + \frac{4.70 \cdot 3.906 - 4.90 \cdot 2.857}{2} = 9.32 \text{ cm}$$

Hence, the transformed point of the liver is (-8.33, 39.39, 9.32).

Step 4: Reorient Phantom

To model the phantom in the treatment planning system, we reorient our phantom to head-first, supine (HFS). Thus, the y- and z-coordinates are reversed. This results in the patient's left to right orientation toward –x direction, superior to inferior orientation toward –z direction, and anterior to posterior orientation toward +y direction. An example of the calculated point of the liver in HFS orientation is presented below.

(-8.33, 39.39, 9.32) y and z are flipped → (-8.33, 9.32, -39.39)

All organ points and body region corner points are reoriented in the same manner.

Steps 5, 6, and 7: Convert Body Regions and Organs to ROI/DICOM format and Plot Phantom in RayStation

After the data are oriented in the HFS coordinate system, each body region is converted from a collection of points to ROI format. Likewise, the collection of points representing an organ is converted to ROI format. Next, the body regions and organs are plotted in RayStation. RayStation allows users to export the phantom in DICOM format, which can be imported for use in any other TPS.

Appendix B: Scaling of any computational phantom using graphical user interface (GUI) surface in RayStation TPS

We have developed a Graphical User Interface (GUI) application in RayStation TPS, which can scale whole-body CT-based anatomy to any arbitrary ages using our ASF. While the latest version of the GUI is discussed here, several modifications will be made soon to accommodate the need for various phantoms and patient scans. The GUI has five tabs, each of which is independent of one another. All of the scaling are performed in the 'Patient Import, and Scaling' tab described below (shown in Figure 17).

The user first imports the phantom and then performs the scaling. In the import panel, age, type of phantom (MDA, UC/NCI, and ICRP (when implemented)), and sex can be specified to import phantoms from our structure template library in the TPS. This particular step is not required if the user has already imported anatomy through DICOM import functions. In the scaling panel, the user specifies the current age of the phantom and then the final target age of the phantom. The user can further select the type of scaling from the following options: MDA Main, 5^{th}, 25^{th}, 50^{th}, 75^{th}, $95^{th,}$ and 99^{th} percentile. The scaling performed here is very fast as the time required to scale 5 body regions and 52 organs is roughly 1.80 minutes. If we combine that time with the time required to import structures, the total time is roughly 3 minutes.

The GUI is in the evolving stage and further modifications are undergoing in the Howell Lab.

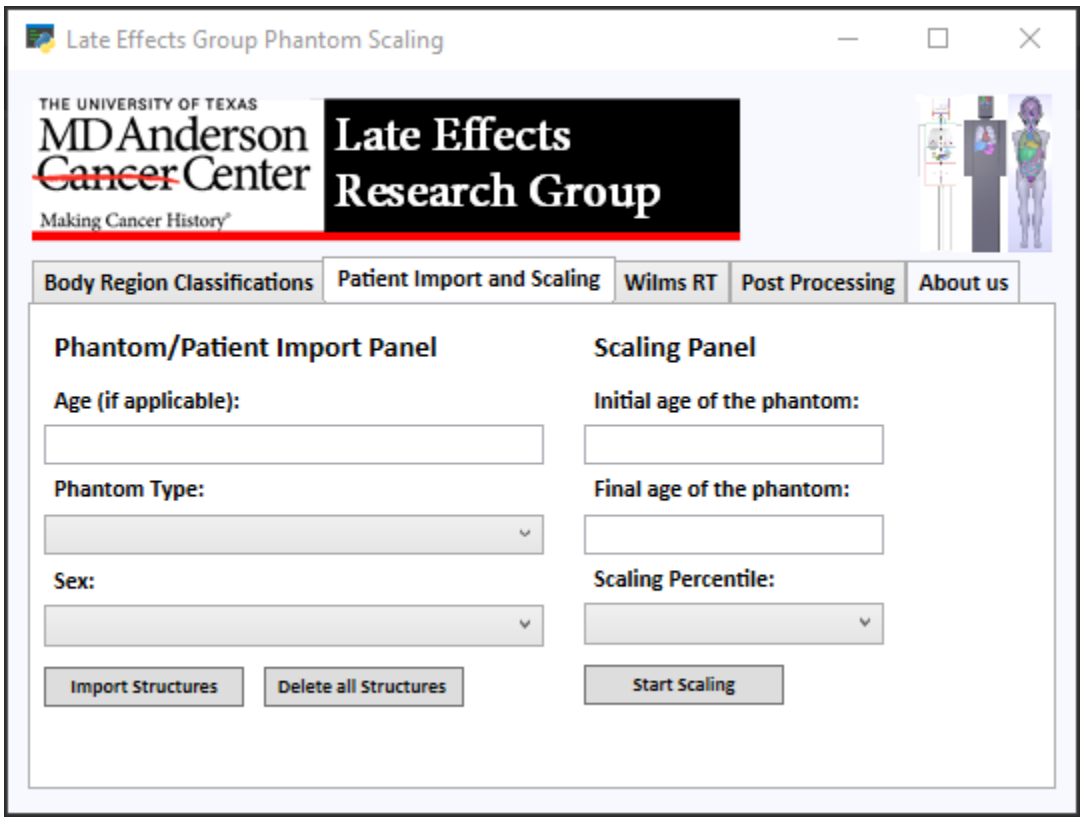

Figure 17: GUI developed in the project to scale computational phantoms to arbitrary ages.

Bibliography

Armstrong G T, Chen Y, Yasui Y, Leisenring W, Gibson T M, Mertens A C, Stovall M, Oeffinger K C, Bhatia S, Krull K R, Nathan P C, Neglia J P, Green D M, Hudson M M and Robison L L 2016 Reduction in Late Mortality among 5-Year Survivors of Childhood Cancer *N. Engl. J. Med.* **374** 833–42

Asdahl P H, Winther J F, Bonnesen T G, De Fine Licht S, Gudmundsdottir T, Anderson H, Madanat-Harjuoja L M, Tryggvadottir L, Smasstuen M, Holmqvist A S, Hasle H and Olsen J H 2015 The Adult Life After Childhood Cancer in Scandinavia (ALiCCS) Study: Design and Characteristics *Pediatr Blood Cancer.* **62** 2204–10

Bates J E, Howell R M, Liu Q, Yasui Y, Mulrooney D A, Dhakal S, Smith S A, Leisenring W M, Indelicato D J, Gibson T M, Armstrong G T, Oeffinger K C and Constine L S 2019 Therapy-related cardiac risk in childhood cancer survivors: An analysis of the childhood cancer survivor study *J. Clin. Oncol.* **37** 1090–101

Bolch W E, Eckerman K, Endo A, Hunt J G S, Jokisch D W, Kim C H, Kim K-P, Lee C, Li J, Petoussi-Henss N, Sato T, Schlattl H, Yeom Y S and Zankl M 2020 *Annals of the ICRP Publication143: Pediatric Reference Computational Phantoms* vol 147

Bolch W, Lee C, Wayson M and Johnson P 2010 Hybrid computational phantoms for medical dose reconstruction *Radiat. Environ. Biophys.* **49** 155–68

Brock K K, Mutic S, McNutt T R, Li H and Kessler M L 2017 Use of image registration and fusion algorithms and techniques in radiotherapy: Report of the AAPM Radiation Therapy Committee Task Group No. 132: Report *Med. Phys.* **44** e43–76

Centers for Disease Control and Prevention N C for H S 2000 *CDC growth charts* Online: https://www.cdc.gov/growthcharts/charts.htm

Davies S C, Hill A L, Holmes R B, Halliwell M and Jackson P C 1994 Ultrasound quantitation of respiratory organ motion in the upper abdomen *Br. J. Radiol.* **67** 1096–102 Online: https://pubmed.ncbi.nlm.nih.gov/7820402/

Dice L R 1945 Measures of the Amount of Ecologic Association Between Species Author (s): Lee R . Dice Published by : Ecological Society of America Stable URL : http://www.jstor.org/stable/1932409 *Ecology* **26** 297–302

Geyer A M, O'Reilly S, Lee C, Long D J and Bolch W E 2014 The UF/NCI family of hybrid computational phantoms representing the current US population of male and female children, adolescents, and adults - Application to CT dosimetry *Phys. Med. Biol.* **59** 5225–42

Gibson T M, Mostoufi-Moab S, Stratton K L, Leisenring W M, Barnea D, Chow E J, Donaldson S S, Howell R M, Hudson M M, Mahajan A, Nathan P C, Ness K K, Sklar C A, Tonorezos E S, Weldon C B, Wells E M, Yasui Y, Armstrong G T, Robison L L and Oeffinger K C 2018 Temporal patterns in the risk of chronic health conditions in survivors of childhood cancer diagnosed 1970–99: a report from the Childhood Cancer Survivor Study cohort *Lancet Oncol.* **19** 1590–601 Online: http://dx.doi.org/10.1016/S1470-2045(18)30537-0

De Gonzalez A B, Curtis R E, Kry S F, Gilbert E, Lamart S, Berg C D, Stovall M and Ron E 2011 Proportion of second cancers attributable to radiotherapy treatment in adults: A cohort study in the US SEER cancer registries *Lancet Oncol.* **12** 353–60 Online:

http://dx.doi.org/10.1016/S1470-2045(11)70061-4

Griffin K T, Mille M M, Pelletier C, Gopalakrishnan M, Jung J W, Lee C, Kalapurakal J, Pyakuryal A and Lee C 2019 Conversion of computational human phantoms into DICOM-RT for normal tissue dose assessment in radiotherapy patients *Phys. Med. Biol.* **64**

Gupta A C, Shrestha S, Owens C A, Smith S A, Qiao Y, Weathers R E, Balter P A, Kry S F and Howell R M 2020 Development of an age-scalable 3D computational phantom in DICOM standard for late effects studies of childhood cancer survivors *Biomed. Phys. Eng. Express* **6**

Haddy N, Diallo S, El-Fayech C, Schwartz B, Pein F, Hawkins M, Veres C, Oberlin O, Guibout C, Pacquement H, Munzer M, N'Guyen T D, Bondiau P Y, Berchery D, Laprie A, Scarabin P Y, Jouven X, Bridier A, Koscielny S, Deutsch E, Diallo I and De Vathaire F 2016 Cardiac diseases following childhood cancer treatment: Cohort study *Circulation* **133** 31–8

Henderson T O, Oeffinger K C, Whitton J, Leisenring W, Neglia J, Meadows A, Crotty C, Rubin D T, Diller L, Inskip P, Smith S A, Stovall M, Constine L S, Hammond S, Armstrong G T, Robison L L and Nathan P C 2012 Secondary gastrointestinal cancer in childhood cancer survivors: A cohort study *Ann. Intern. Med.* **156** 757–66

Howell R M, Scarboro S B and Taddei P J 2010a Accuracy of out-of-field dose calculations by a commercial treatment planning system *Phys. Med. Biol. To* **55** 6999

Howell R M, Scarboro S B, Taddei P J, Krishnan S, Kry S F and Newhauser W D 2010b Methodology for determining doses to in-field, out-of-field and partially in-field organs for late effects studies in photon radiotherapy *Phys. Med. Biol.* **55** 7009–23

Howell R M, Smith S A, Weathers R E, Kry S F and Stovall M 2019 Adaptations to a Generalized Radiation Dose Reconstruction Methodology for Use in Epidemiologic Studies: An Update from the MD Anderson Late Effect Group *Radiat. Res.* **192** 169–88

Howlader N, AM N, M K, D M, A B, M Y, J R, Z T, A M, DR L, HS C, EJ F and KA C 2019 *SEER Cancer Statistics Review (CSR) 1975-2018* (Bethesda)

Hudson M M, Ehrhardt M J, Bhakta N, Baassiri M, Eissa H, Chemaitilly W, Green D M, Mulrooney D A, Armstrong G T, Brinkman T M, Klosky J L, Krull K R, Sabin N D, Wilson C L, Huang I C, Bass J K, Hale K, Kaste S, Khan R B, Srivastava D K, Yasui Y, Joshi V M, Srinivasan S, Stokes D, Hoehn M E, Wilson M, Ness K K and Robison L L 2017 Approach for classification and severity grading of long-term and late-onset health events among childhood cancer survivors in the St. Jude lifetime cohort *Cancer Epidemiol. Biomarkers Prev.* **26** 666–74

Hudson M M, Ness K K, Nolan V G, Armstrong G T, Green D M, Morris E B, Spunt S L, Metzger M, Krull K R, Klosky J L, Srivastava D K and Robison L L 2011 Prospective Medical Assessment of Adults Surviving Childhood Cancer: Study Design, Cohort Characteristics, and Feasibility of the St. Jude Lifetime Cohort Study *Pediatr Blood Cancer.* **23** 1–7 Online: https://www.ncbi.nlm.nih.gov/pmc/articles/PMC3624763/pdf/nihms412728.pdf

Huelke D F 1998 An Overview of Anatomical Considerations of Infants and Children in the Adult World of Automobile Safety Design *J. Biomech.* **2** 267–80

ICRP 2002 ICRP 89 - Basic Anatomical and Physiological Data for Use in Radiological Protection: Reference Values *Ann. ICRP*

ICRU 1992a *ICRU Report 48: Phantoms and computational models in therapy, diagnosis and protection* vol 1 (Bethesda)

ICRU 1992b *Photon, Electron, Proton and Neutron Interaction Data for Body Tissues* (Bethesda)

Johnson P, Juneja B, Lee C and Bolch W 2009 TU-E-304A-01: Hybrid Patient-Dependent Phantoms Covering Statistical Distributions of Body Morphometry in the U.S. Adult Population: Development and Validation *Med. Phys.* **36** 2747

Kalapurakal J A, Gopalakrishnan M, Mille M, Helenowski I, Peterson S, Rigsby C, Laurie F, Jung J W, Fitzgerald T J and Lee C 2018 Feasibility and accuracy of UF/NCI phantoms and Monte Carlo retrospective dosimetry in children treated on National Wilms Tumor Study protocols *Pediatr. Blood Cancer* **65** 1–8

Kim C H, Yeom Y S, Petoussi-Henss N, Zankl M, Bolch W E, Lee C, Choi C, Nguyen T T, Eckerman K, Kim H S, Han M C, Qiu R, Chung B S, Han H and Shin B 2020 *Annals of the ICRP Publication 145: Adult Mesh-Type Reference Computational Phantoms* vol 49

Kry S F, Bednarz B, Howell R M, Dauer L, Followill D, Klein E, Paganetti H, Wang B, Wuu C S and George Xu X 2017 AAPM TG 158: Measurement and calculation of doses outside the treated volume from external-beam radiation therapy *Med. Phys.* **44** e391–429

Kry S F, Followill D, White R A, Stovall M, Kuban D A and Salehpour M 2007 Uncertainty of Calculated Risk Estimates for Secondary Malignancies After Radiotherapy *Int. J. Radiat. Oncol. Biol. Phys.* **68** 1265–71

Kutanzi K R, Lumen A, Koturbash I and Miousse I R 2016 Pediatric Exposures to Ionizing

Radiation: Carcinogenic Considerations *Int. J. Environ. Res. Public Health* **13**

Kuzmin G A, Mille M M, Jung J W, Lee C, Pelletier C, Akabani G and Lee C 2018 A Novel Method to Extend a Partial-Body CT for the Reconstruction of Dose to Organs beyond the Scan Range *Radiat. Res.* **189** 618–26

Langen K M and Jones D T L 2001 Organ motion and its management *Int. J. Radiat. Oncol. Biol. Phys.* **50** 265–78

Lee C, Lee C and Bolch W E 2006 Age-dependent organ and effective dose coefficients for external photons: A comparison of stylized and voxel-based paediatric phantoms *Phys. Med. Biol.* **51** 4663–88

Lee C, Lodwick D, Hurtado J, Pafundi D, Williams J L and Bolch W E 2010 The UF family of reference hybrid phantoms for computational radiation dosimetry *Phys. Med. Biol.* **55** 339–63

Leisenring W M, Mertens A C, Armstrong G T, Stovall M A, Neglia J P, Lanctot J Q, Boice J D, Whitton J A and Yasui Y 2009 Pediatric cancer survivorship research: Experience of the childhood cancer survivor study *J. Clin. Oncol.* **27** 2319–27

Mattiucci G C, Boldrini L, Chiloiro G, D'Agostino G R, Chiesa S, De Rose F, Azario L, Pasini D, Gambacorta M A, Balducci M and Valentini V 2013 Automatic delineation for replanning in nasopharynx radiotherapy: What is the agreement among experts to be considered as benchmark? *Acta Oncol. (Madr).* **52** 1417–22

Molina D K, Pinneri K, Stash J A, Li L, Vance K and Cross C 2019 Organ Weight Reference Ranges for Ages 0 to 12 Years **40** 318–28

Morton L M, Dores G M, Curtis R E, Lynch C F, Stovall M, Hall P, Gilbert E S, Hodgson D C, Storm H H, Johannesen T B, Smith S A, Weathers R E, Andersson M, Fossa S D, Hauptmann M, Holowaty E J, Joensuu H, Kaijser M, Kleinerman R A, Langmark F, Pukkala E, Vaalavirta L, Van Den Belt-Dusebout A W, Fraumeni J F, Travis L B, Aleman B M and Van Leeuwen F E 2013 Stomach cancer risk after treatment for Hodgkin lymphoma *J. Clin. Oncol.* **31** 3369–77

Mulrooney D A, Yeazel M W, Kawashima T, Mertens A C, Mitby P, Stovall M, Donaldson S S, Green D M, Sklar C A, Robison L L and Leisenring W M 2009 Cardiac outcomes in a cohort of adult survivors of childhood and adolescent cancer: Retrospective analysis of the childhood cancer survivor study cohort *BMJ* **339** 34

Nottage K, McFarlane J, Krasin M J, Li C, Srivastava D, Robison L L and Hudson M M 2012 Secondary colorectal carcinoma after childhood cancer *J. Clin. Oncol.* **30** 2552–8

ORNL 1966 *Variation of dose delivered by 137Cs as a function of body size from infancy to adulthood*

Robison L L, Armstrong G T, Boice J D, Chow E J, Davies S M, Donaldson S S, Green D M, Hammond S, Meadows A T, Mertens A C, Mulvihill J J, Nathan P C, Neglia J P, Packer R J, Rajaraman P, Sklar C A, Stovall M, Strong L C, Yasui Y and Zeltzer L K 2009 The childhood cancer survivor study: A national cancer institute-supported resource for outcome and intervention research *J. Clin. Oncol.* **27** 2308–18

Segars W P, Sturgeon G, Mendonca S, Grimes J and Tsui B M W 2010 4D XCAT phantom for multimodality imaging research *Med. Phys.* **37** 4902–15

Shrestha S, Gupta A C, Bates J E, Lee C, Owens C A, Hoppe B S, Constine L S, Smith S A, Qiao Y, Weathers R E, Yasui Y, Court L E, Paulino A C, Pinnix C C, Kry S F, Followill D S, Armstrong G T and Howell R M 2020 Development and validation of an age-scalable cardiac model with substructures for dosimetry in late-effects studies of childhood cancer survivors *Radiother. Oncol.* **153** 163–71 Online: https://doi.org/10.1016/j.radonc.2020.10.017

Snyder R G, Schneider L W, Owings C L, Reynolds H M, Golomb D H and Schork M A 1977 *Anthropometry of Infants, Children, and Youths to Age 18 for Product Safety Design SP450* (Warrendale, PA)

Stovall M, Weathers R, Kasper C, Smith S A, Travis L, Ron E and Kleinerman R 2006 Dose reconstruction for therapeutic and diagnostic radiation exposures: Use in epidemiological studies *Radiat. Res.* **166** 141–57

Suramo I, Paivansalo M and Myllyla V 1984 Cranio-Caudal movements of the liver, pancreas, and kidneys in respiration *Acta radiol.* **25** 129–30

Teepen J C, Kremer L C M, Ronckers C M, Van Leeuwen F E, Hauptmann M, Van Dulmen-Den Broeder E, Van Der Pal H J, Jaspers M W M, Tissing W J, Van Den Heuvel-Eibrink M M, Loonen J J, Bresters D, Versluys B, Visser O, Neggers S J C M M and Van Der Heiden-Van Der Loo M 2017 Long-term risk of subsequent malignant neoplasms after treatment of childhood cancer in the DCOG LATER study cohort: Role of chemotherapy *J. Clin. Oncol.* **35** 2288–98

Thomson D, Boylan C, Liptrot T, Aitkenhead A, Lee L, Yap B, Sykes A, Rowbottom C and Slevin N 2014 Evaluation of an automatic segmentation algorithm for definition of head and

neck organs at risk *Radiat. Oncol.* **9** 1–12

Travis L B, Boice J D, Alan J M and Applegate K E 2011 *Second Primary Cancers and Cardiovascular Disease after Radiation Therapy. NCRP Report No. 170.* vol 39

Tukenova M, Diallo I, Anderson H, Hawkins M, Garwicz S, Sankila R, El Fayech C, Winter D, Rubino C, Adjadj E, Haddy N, Oberlin O, Moller T, Langmark F, Tryggvadottir L, Pacquement H, Svahn-Tapper G and De Vathaire F 2012 Second malignant neoplasms in digestive organs after childhood cancer: A cohort-nested case-control study *Int. J. Radiat. Oncol. Biol. Phys.* **82**

Turcotte L M, Liu Q, Yasui Y, Arnold M A, Hammond S, Howell R M, Smith S A, Weathers R E, Henderson T O, Gibson T M, Leisenring W, Armstrong G T, Robison L L and Neglia J P 2017 Temporal trends in treatment and subsequent neoplasm risk among 5-year survivors of childhood cancer, 1970-2015 *JAMA - J. Am. Med. Assoc.* **317** 814–24

Vũ Bezin J, Allodji R S, Mège J P, Beldjoudi G, Saunier F, Chavaudra J, Deutsch E, De Vathaire F, Bernier V, Carrie C, Lefkopoulos D and Diallo I 2017 A review of uncertainties in radiotherapy dose reconstruction and their impacts on dose-response relationships *J. Radiol. Prot.* **37** R1–18

Van Der Walt S, Schönberger J L, Nunez-Iglesias J, Boulogne F, Warner J D, Yager N, Gouillart E and Yu T 2014 Scikit-image: Image processing in Python *PeerJ* **2014** 1–18

Whalen S, Lee C, Williams J L and Bolch W E 2008 Anthropometric approaches and their uncertainties to assigning computational phantoms to individual patients in pediatric dosimetry studies *Phys. Med. Biol.* **53** 453–71

Xie T and Zaidi H 2014 Evaluation of radiation dose to anthropomorphic paediatric models from positron-emitting labelled tracers *Phys. Med. Biol.* **59** 1165–87

Xu X G 2014 An exponential growth of computational phantom research in radiation protection, imaging, and radiotherapy: A review of the fifty-year history *Phys. Med. Biol.* **59**

Xu X G, Bednarz B and Paganetti H 2008 A review of dosimetry studies on external-beam radiation treatment with respect to second cancer induction *Phys. Med. Biol.* **53**

Zaidi H and Tsui B M W 2009 Review of computational anthropomorphic anatomical and physiological models *Proc. IEEE* **97** 1938–53

Zou K H, Warfield S K, Bharatha A, Tempany C M C, Kaus M R, Haker S J, Wells W M, Jolesz F A and Kikinis R 2004 Statistical validation of image segmentation quality based on a spatial overlap index *Acad. Radiol.* **11** 178–89

Vita

Aashish Chandra Gupta was born in Nepal on February 7, 1994, the son of Dinesh Chandra Gupta and Punam Gupta. After completing his high school at Universal Academy, Janakpur, Nepal, he entered Texas Tech University in 2016. He received the degree of Bachelor of Science with a major in Physics in May 2018. In July of 2018, he entered the Medical Physics Program at The University of Texas MD Anderson Cancer Center UTHealth Graduate School of Biomedical Sciences.

Permanent address:

7900 Cambridge Street, APT 4-1E

Houston, TX 77054